REPORT SAMSO TR-78-30

LEVEL II

12

Laser Irradiation of Carbon Fibers and Composites

J. STEPHEN EVANGELIDES
Development Group
The Aerospace Corporation
El Segundo, Calif. 90245

25 January 1979

Final Report

Prepared for

SPACE AND MISSILE SYSTEMS ORGANIZATION
AIR FORCE SYSTEMS COMMAND
Los Angeles Air Force Station
P.O. Box 92960, Worldway Postal Center
Los Angeles, Calif. 90009

This final report was submitted by The Aerospace Corporation, El Segundo, California 90245, under Contract F04701-78-C-0079 with the Space and Missile Systems Organization, Deputy for Reentry Systems, P.O. Box 92960, Worldway Postal Center, Los Angeles California, 90009. It was reviewed and approved for The Aerospace Corporation by W. C. Riley, Laboratory Operations, and R. B. Mortensen, Reentry Systems Division, Development Group. Capt J. W. Bohlen was the project engineer.

This report has been reviewed by the Information Office (OI) and is releasable to the National Technical Information Service (NTIS). At NTIS, it will be available to the general public, including foreign nations.

This technical report has been reviewed and is approved for publication. Publication of this report does not constitute Air Force approval of the report's findings or conclusions. It is published only for the exchange and stimulation of ideas.

James W. Bohlen
Capt, USAF
Project Officer

James M. McCormack
Lt Col, USAF
Chief, Reentry Technology Division

W. Goldberg
Col, USAF
Chief, Systems Technology Directorate

UNCLASSIFIED

SECURITY CLASSIFICATION OF THIS PAGE (When Data Entered)

REPORT DOCUMENTATION PAGE	READ INSTRUCTIONS BEFORE COMPLETING FORM
1. REPORT NUMBER: SAMSO TR-78-30	2. GOVT ACCESSION NO. / 3. RECIPIENT'S CATALOG NUMBER
4. TITLE (and Subtitle): LASER IRRADIATION OF CARBON FIBERS AND COMPOSITES,	5. TYPE OF REPORT & PERIOD COVERED: Final Report.
	6. PERFORMING ORG. REPORT NUMBER: TR-0079(4550-75)-1
7. AUTHOR(s): J. Stephen Evangelides	8. CONTRACT OR GRANT NUMBER(s): F04701-78-C-0079
9. PERFORMING ORGANIZATION NAME AND ADDRESS: The Aerospace Corporation, El Segundo, California 90245	10. PROGRAM ELEMENT, PROJECT, TASK AREA & WORK UNIT NUMBERS
11. CONTROLLING OFFICE NAME AND ADDRESS: Space and Missile Systems Organization, Air Force Systems Command, Los Angeles, California 90009	12. REPORT DATE: 25 Jan 1979 / 13. NUMBER OF PAGES: 84
14. MONITORING AGENCY NAME & ADDRESS (if different from Controlling Office): 81 p.	15. SECURITY CLASS. (of this report): UNCLASSIFIED / 15a. DECLASSIFICATION/DOWNGRADING SCHEDULE

16. DISTRIBUTION STATEMENT (of this Report)

APPROVED FOR PUBLIC RELEASE; DISTRIBUTION UNLIMITED

17. DISTRIBUTION STATEMENT (of the abstract entered in Block 20, if different from Report)

18. SUPPLEMENTARY NOTES

19. KEY WORDS (Continue on reverse side if necessary and identify by block number)

Carbon-Carbon Composites
Carbon Fibers
Carbon Polymorphs
Laser Irradiation
Microstructure
Rocket Nozzle

20. ABSTRACT (Continue on reverse side if necessary and identify by block number)

The use of carbon-carbon composites as reentry vehicle nose tips has increased due to their unique thermochemical and thermostructural properties. One performance criterion of particular importance to the aerospace community is the ablation behavior. Since a large number of candidate composites is available, a preliminary screening test was sought which could select the most promising fibers and composites. Therefore, the objective of this program was to irradiate various carbon/graphite filaments, bulk pitch matrices, carbon-carbon composites and pyrolytic graphite to characterize mass loss

DD FORM 1473 (FACSIMILE)

004 500

UNCLASSIFIED

SECURITY CLASSIFICATION OF THIS PAGE (When Data Entered)

19. KEY WORDS *(Continued)*

20. ABSTRACT *(Continued)*

and structural changes. The laser irradiation experiments have provided an insight into the microstructural mechanisms of ablation. They have shown that correlations exist between mass loss and material properties, that differences exist in mass loss characteristics between composite constituents, and that ablation testing results in similar correlations. It was concluded that laser irradiation of reentry nose tip materials can be used to investigate the behavior of carbonaceous materials in an ablation environment.

LEVEL II

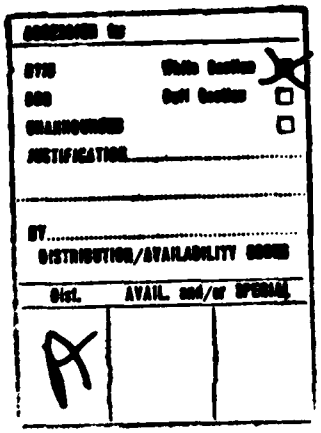

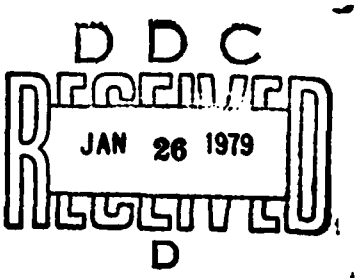

PREFACE

The author wishes to acknowledge the encouragement and sponsorship of Lt Col J. McCormack, SAMSO (RSSE). The valuable contribution of Dr. J. Lundell of NASA, AMES, in assisting in the laser irradiation experiments is appreciated. The author is indebted to A. G. Whittaker and P. L. Kintner for testing, to J. R. Van Landingham for specimen preparation, to T. G. Espinosa and K. E. Wrightsel for optical and scanning electron microscopy, and to G. S. Rellick for editing the final manuscript.

CONTENTS

TABLES

FIGURES

FIGURES (Continued)

FIGURES (Continued)

I. INTRODUCTION

The advent of advanced missile systems with increased performance requirements has necessitated the development and use of carbon-carbon composites for reentry vehicle nose tips. Two material properties of importance in a reentry environment are recession rate and transition altitude. Since a variety of precursor materials (fibers and matrices), reinforcement constructions (orthogonal, polar, and seven-directional), and processing methods (high and low pressure) exist, a large number of candidate composites is available. Unfortunately, ablation tests are both expensive and time-consuming in that composites must be fabricated and models machined and tested. Although the tests have been informative and the data have been useful, the results have also been confusing, if not conflicting. Therefore, a preliminary screening test was sought which could provide a means of selecting the most promising fibers and composites in an economical and expedient manner.

According to studies of events occurring during reentry, sublimation (vaporization and particle emission) was the primary mechanism of mass loss.[1,2] Heat fluxes typical of reentry, 30,000 (laminar flow) to 80,000 (turbulent flow) (Btu/ft^2)/sec could be obtained from a CO_2 laser in the absence of strong aerodynamic flow. In addition to evaluating a screening criterion, this test could provide ablated surfaces for studying the mechanisms of ablation. Therefore, the objective of this program was to study the mass loss characteristics of various precursor materials and composites by laser irradiation. The experimental approach was to irradiate various carbon/graphite filaments and pyrolytic graphite (PG) in both the

[1] K. Kratsch, Personal Communication, Science Applications, Inc. (May 1976).

[2] A. G. Whittaker and P. L. Kintner, Particle Emission and Related Morphological Changes Occurring During the Sublimation of Graphitic Carbons, 14, 257 (1976).

longitudinal and transverse directions, and bulk pitch matrix and carbon-carbon composites in one direction. Total mass loss was measured after each exposure and the irradiated surfaces were characterized by optical and scanning electron microscopy (SEM). Through this type of study, the merits of a mass loss criterion could be evaluated and a significant contribution to the knowledge of carbon ablation mechanisms might be made.

A search of the open literature indicated that data on mass loss due to sublimation in carbon fibers were totally lacking. One study conducted by Barnet and Norr investigated the structural aspects of carbon/graphite filaments after oxygen plasma etching, but not the mass loss characteristics.[3] The results of that study supported the "circumferential-radial" mode for high modulus polacrylonitrile (PAN) and the "onion skin" structural model for high modulus rayon.

[3] F. R. Barnet and M. K. Norr, "Carbon Fiber Etching in an Oxygen Plasma," Carbon, Vol. 11, 281-288 (1973).

II. MATERIALS

The two principal precursor materials currently used in carbon fiber fabrication for reentry applications are PAN and petroleum pitch. Primary examples are designated HM2000 by Hercules, Inc., and Thornel P by Union Carbode Corporation, respectively. However, to achieve the stated objectives of this program, a wide spectrum of precursor materials was needed. Therefore, in addition to these two filaments, six additional filaments were selected, including three rayon precursor filaments (see Table 1).

The reference material for these experiments was pyrolytic graphite (PG). This served as a valuable control because it represented extremes in crystallographic orientation which were present in the filaments. In addition, the C-direction of the PG also provided a suitable representation of the pitch matrix sheath which surrounds the filaments in a carbon-carbon composite processed by low-pressure impregnation procedures. To complete the matrix structures to be evaluated, samples of bulk coal tar pitch (Allied Chemical Corporation 277-15V) processed by low (1000 psi) and high (15,000 psi) impregnation pressures were obtained.[4] The bulk matrix processed at high pressure was also taken to represent the inter-filament matrix in a composite processed by the high-pressure procedures. The final series of specimens were Thornel 50 multidirectional carbon-carbon composites processed by different procedures (see Table 2).

[4] J. S. Evangelides, et al., Carbon Materials Analyses, Report No. TOR-0077(2725-01)-2, The Aerospace Corporation, El Segundo, CA (31 December 1976).

Table 1. Filament Description

(Manufacturer's Data Unless Otherwise Noted)

Specimen	Manufacturer	Precursor	Diameter, μm	Density, g/cc	Tensile Modulus, Msi	Tensile Strength, ksi
WYB	Union Carbide Corp.	Rayon	8.9	1.32	6	90
Thornel 50	Union Carbide Corp.	Rayon	6.6	1.66	57	315
Thornel 75	Union Carbide Corp.	Rayon	6.0	1.80	78	380
Thornel 300	Union Carbide Corp.	PAN	7.6	1.70	34	325
Modmor II	Morganite, Inc.	PAN	8.1	1.71	39	360
HM2000	Hercules, Inc.	PAN	7.5	1.81	54	355
GY 70	Celanese Corp.	PAN	8.4	1.96	75	270
Thornel P[5]	Union Carbide Corp.	Pitch	9.0	1.92	57	154

[5]P. J. Legendre ed., Advanced Fiber Reentry Material Performance Review, Report No. TOR-0077(2550-72)-1, The Aerospace Corporation, El Segundo, CA (28 January 1977).

Table 2. Thornel 50 Composite Descriptions

Material	Manufacturer	Construction*	Process
AX-1	McDonnell Douglas Astronautics Co.	223	Low Pressure Impregnation[6] (1000 psi) - 277-15V Matrix
AX-2	McDonnell Douglas Astronautics Co.		
B1-1	General Electric Company	223	Chemical Vapor Deposition (CVD) and High Pressure Impregnation[7] (15, 000 psi) - 277-15V Matrix
B1-2	General Electric Company		
D2-1	General Electric Company		
D2-2	General Electric Company		
4-1	Fiber Materials, Inc.	221	Mixed Pressure Impregnation[7] (15 + 10, 000 psi) - A240 Matrix**
4-2	Fiber Materials, Inc.		

*Designation indicates the number of fibers in x-direction, y-direction, and z-direction, respectively, of the orthogonal composite.

**Ashland Oil Company.

[6]R. W. Seibold, et al., Exploratory Development and Assessment of Improved Multidirectionally Reinforced Carbon-Carbon Composites, Processed at Pressure to 920 psi, Report No. MDC G6549, McDonnell Douglas Astronautics Company (December 1976).

[7]E. R. Stover, Multidirectional Reinforced Carbon-Carbon Composites for Re-Entry Vehicle Applications, Report No. AFML TR-72-250 D-L III, General Electric Company (March 1976).

III. EXPERIMENTAL PROCEDURE

The filament irradiation tests were conducted on bare, unimpregnated filaments. This required a special holding fixture to permit irradiation in both the longitudinal and transverse directions (Figure 1). The filaments were loaded into the fixtures and compressed by a plate to volume fractions of 0.51 to 0.77. The transverse filament ends were cut with a scalpel to obtain a flat surface. The longitudinal surface did not require any additional handling after loading. Bulk pitch and composite specimens were either cylindrical or rectangular in shape and approximately 1.0 in. in diameter (length) and 0.4 to 1.0 in. in thickness. The surfaces of these specimens were polished with N 600 grit paper to remove any gross machining marks.

The laser irradiation tests were conducted on the 90 kW CO_2 laser at NASA Ames Laboratory. Typical laser power levels and exposure times were 10 kW for 0.5 sec and 5 kW for 1.0 sec, except for the transverse filament direction where a 10 kW power level was used. These exposure levels were selected from preliminary tests which indicated that specimen burn-throughs would not occur at these levels. Two different exposure times were sought in order to estimate a mass loss rate. A flow of argon was maintained over the specimen surface to reduce the amount of carbon vapor that was re-depositing on the specimen surface. The temperatures for all tests were measured by an optical pyrometer. Specimen temperatures varied between 3700° and 4100°C. Obtaining consistently accurate temperature measurements was difficult due to sighting and fogging problems. However, temperatures were found to vary between specimens due to slight changes in laser power and also during an exposure due to laser fluctuations. This was confirmed by the pictures which were taken of each test.

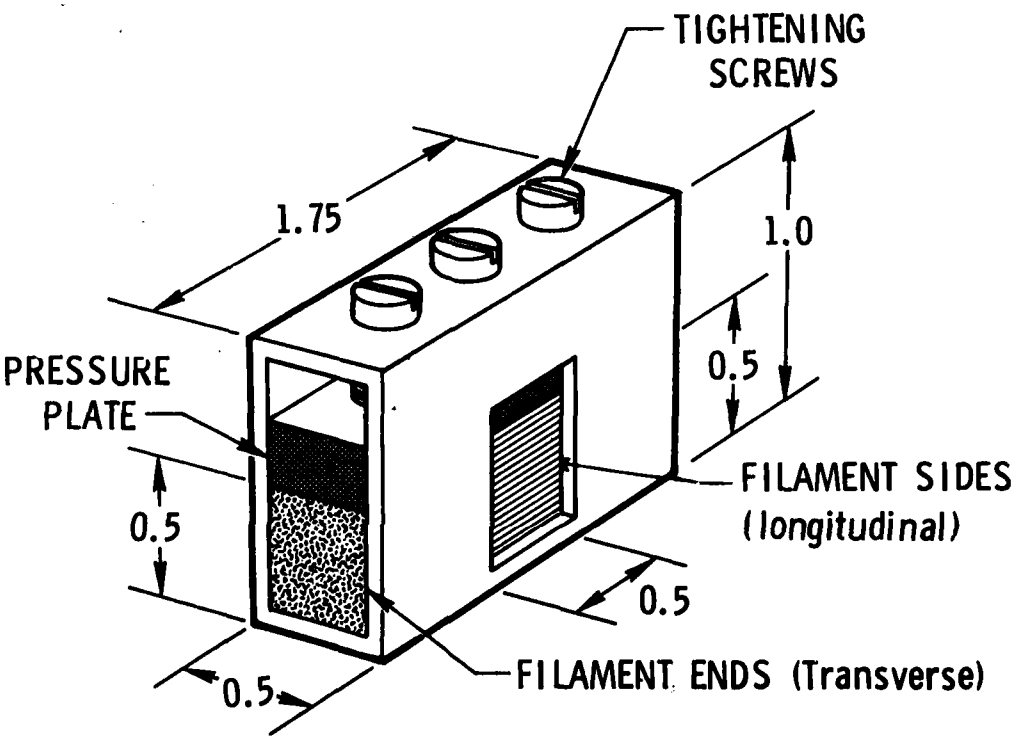

NOTE: All dimensions are given in inches

Figure 1. Filament-Holding Fixture (Material: Steel)

Weight loss was determined after each test. Specimen damage was characterized by optical and scanning electron microscopy. The composite specimens were cross-sectioned through the center of the crater to investigate in-depth material changes. All specimen weight loss and exposure conditions are tabulated in the Appendix. Five longitudinal filament exposures were discarded due to improper beam alignment which resulted in the edge of the holding fixture being irradiated.

IV. EXPERIMENT RESULTS

A. MASS LOSS

The mass loss data were analyzed with respect to laser power and energy to examine the effects on material property relationships. For these experiments the cross-sectioned area of the laser beam was assumed to be constant. Upon calculating the mass loss per deposited energy, it was noticed that the 0.5-sec exposures were generally higher than the 1.0-sec exposures (see Table 3). These higher initial mass loss rates were thought to be due to the initial thermal shock causing microfracturing, resulting in local spallation and mass removal. Therefore, an equilibrium rate would be obtained only after an initial induction period. This was particularly true for the composite and matrix specimens where the 0.5-sec rates were 37 percent greater than the 1.0-sec rates.

Filament mass loss was divided by laser power and plotted against the time of exposure for each filament (see Figures 2 thru 6). The linear regression analyses of the data resulted in strong correlations in all but a few cases (see Table 4). As expected, irradiation in the transverse filament direction resulted in a greater mass loss than irradiation in the longitudinal direction. Initially, there was concern that, since the filament volume fraction varied from 51 to 77 percent between filament holders, any relationships with mass loss would be obscured or altered. However, the correlation factors between mass loss and filament volume fraction and effective bulk density (filament volume fraction times filament density) were poor, being only 0.57 and -0.23, respectively. Therefore, even though filament volume fraction is expected to influence mass loss, it was secondary to the large differences in filament modulus, density, and crystallographic orientation. The filament volume fractions were calculated from the volume of the holder, filament density, and filament mass (see Table 5).

Table 3. Summary of Mass Loss per Deposited Energy for Two Exposure Times

System	Direction	Mass Loss per Energy Deposited		
		0.5 sec	1.0 sec	Difference*, %
WYB	Transverse	22.2	18.1	18
Thornel 50		15.4	14.6	5
Thornel 75		9.8	11.1	-13
Thornel 300		23.0	17.8	23
Modmor II		13.5	13.2	2
HM2000		17.8	13.0	28
GY 70		13.1	11.4	13
Thornel P		18.0	14.2	21
WYB	Longitudinal	9.9	—	—
Thornel 50		—	8.4	—
Thornel 75		8.0	—	—
Thornel 300		14.0	14.2	- 1
Modmor II		10.2	6.7	34
HM 2000		9.2	8.1	12
GY 70		7.5	—	—
Thornel P		8.7	8.4	35
PG	c	2.0	2.1	- 5
	a	1.3	1.7	-31
GE 223	z	4.3	—	—
MDAC 223	z	2.1	1.5	29
FMI 221	z	4.3	1.7	60
HiPIC	—	5.5	4.9	11
LoPIC	—	10.3	5.4	48

*Differences between 0.5-sec and 1.0-sec mass losses.

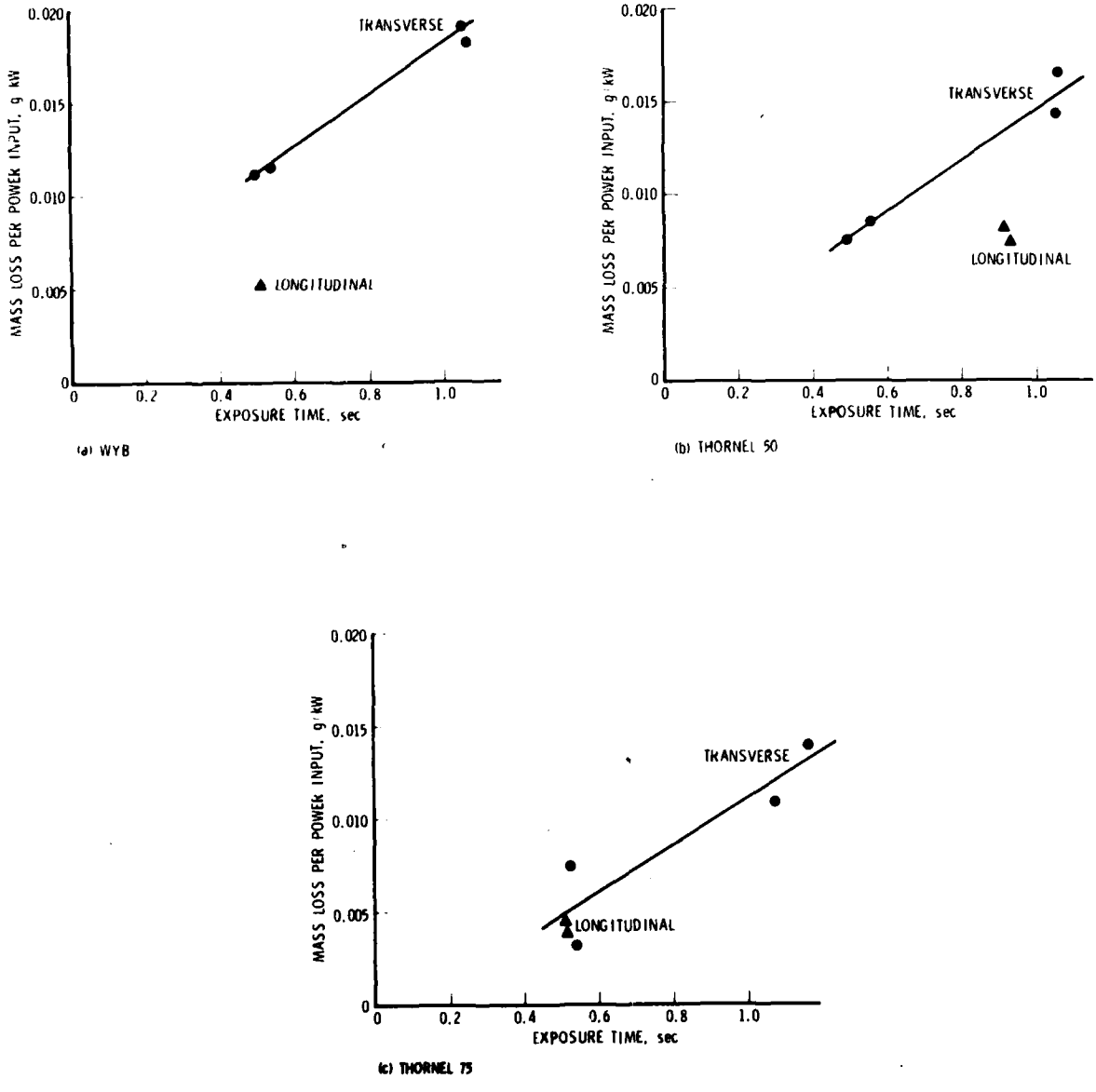

Figure 2. Transverse and Longitudinal Mass Losses for Rayon Precursor Filaments

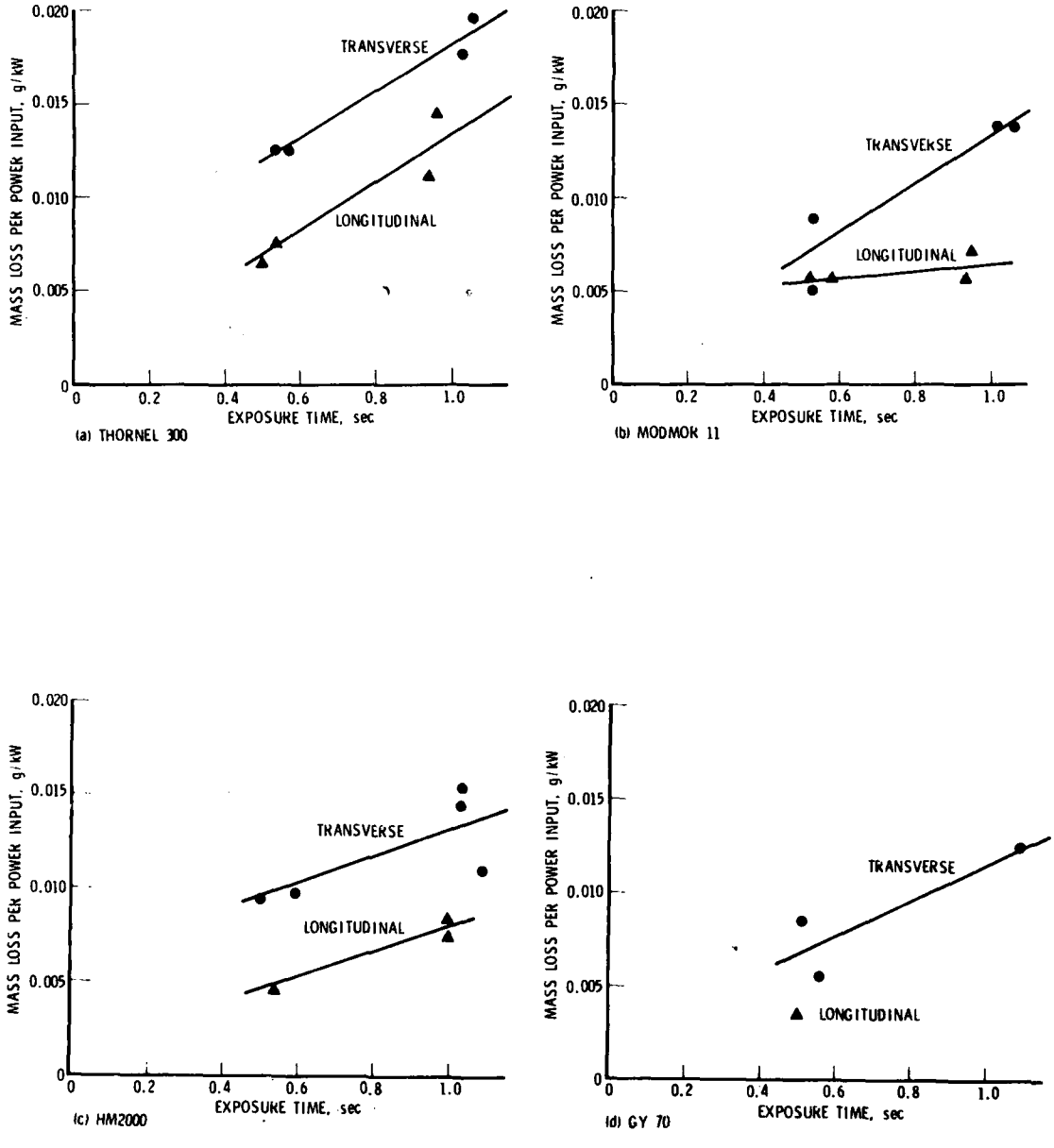

Figure 3. Transverse and Longitudinal Mass Loss for Polyacrylonitrile Precursor Filaments

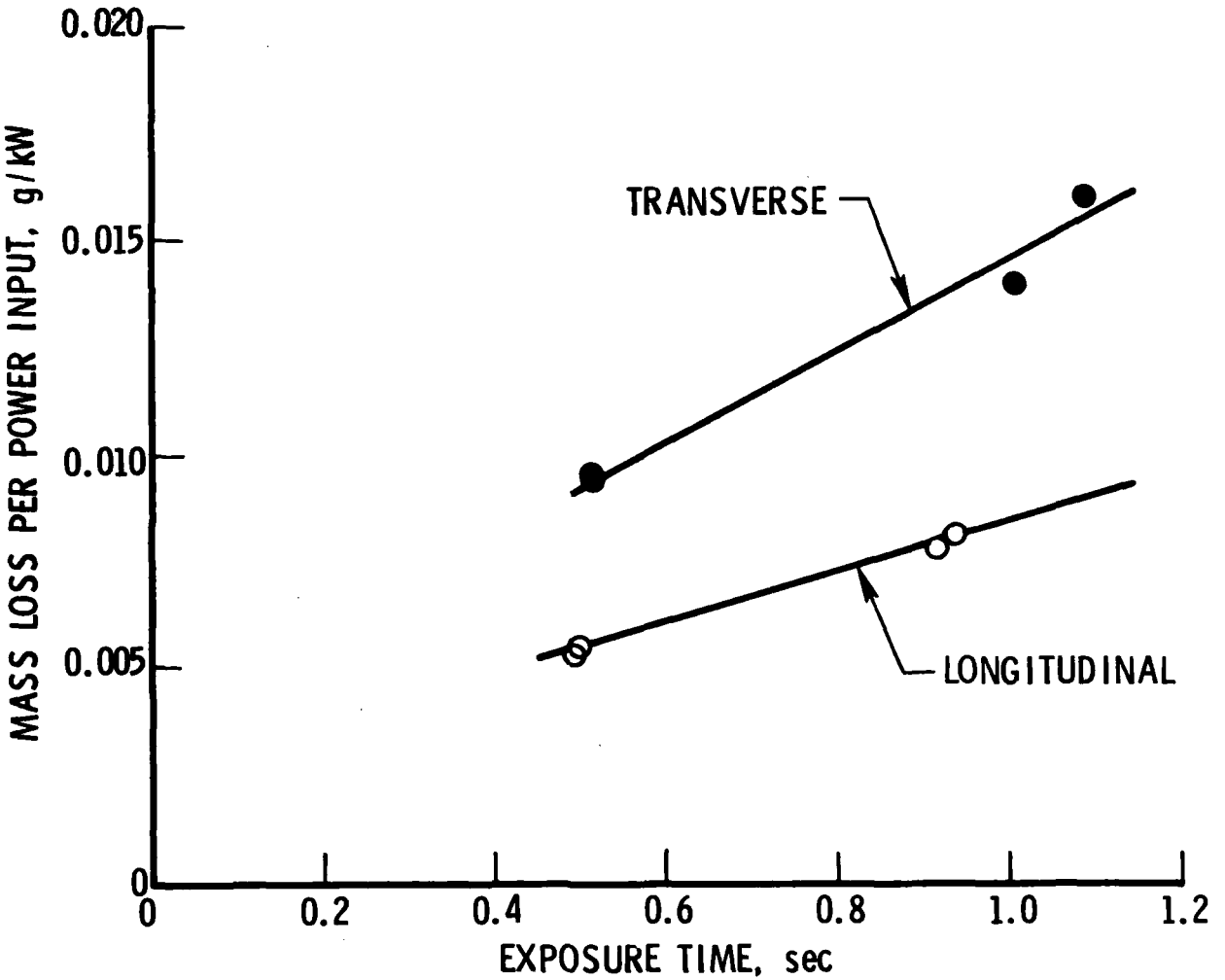

Figure 4. Transverse and Longitudinal Mass Loss Data for Pitch Precursor Filaments

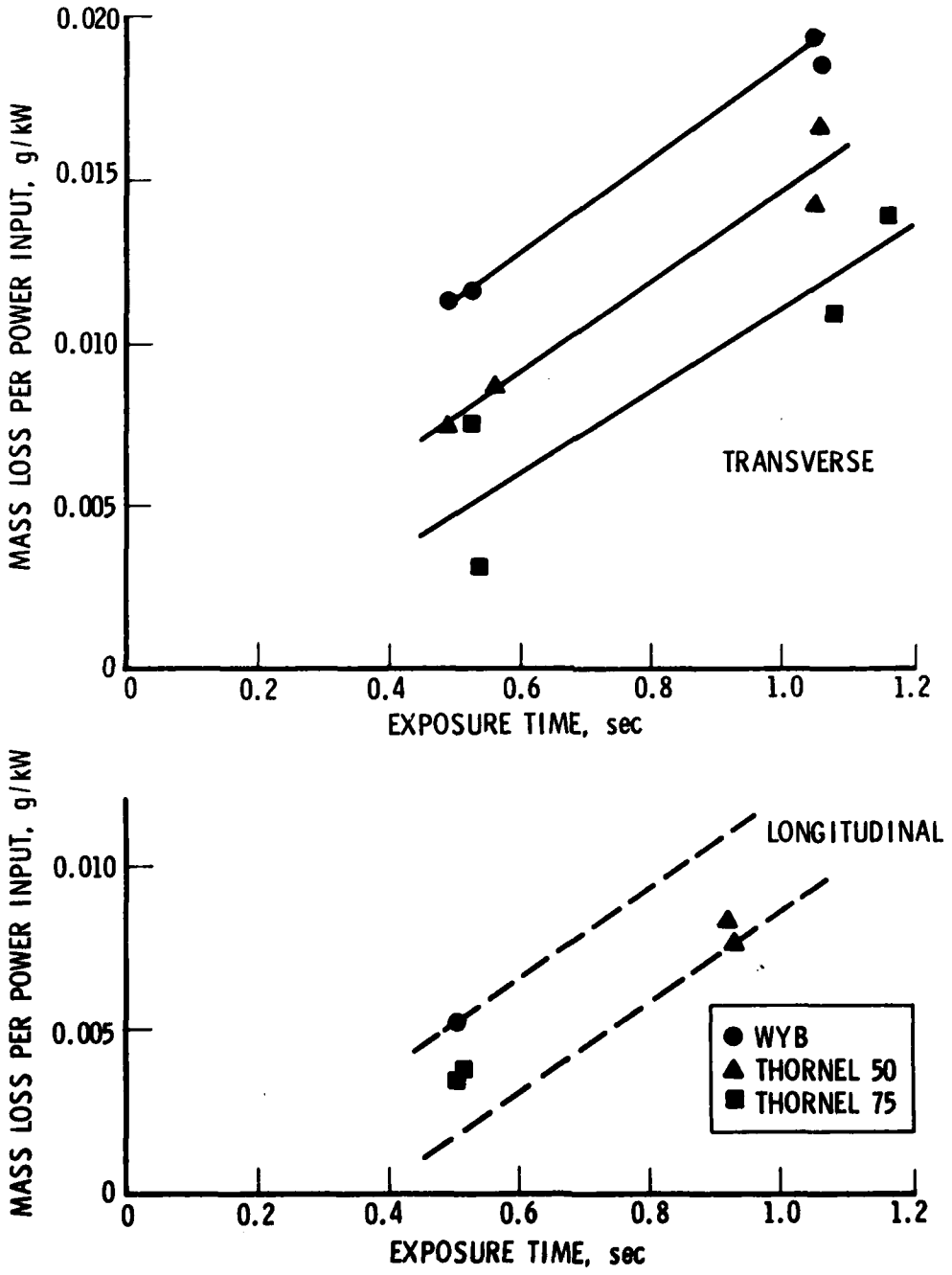

Figure 5. Mass Loss Data for Rayon Precursor Filaments

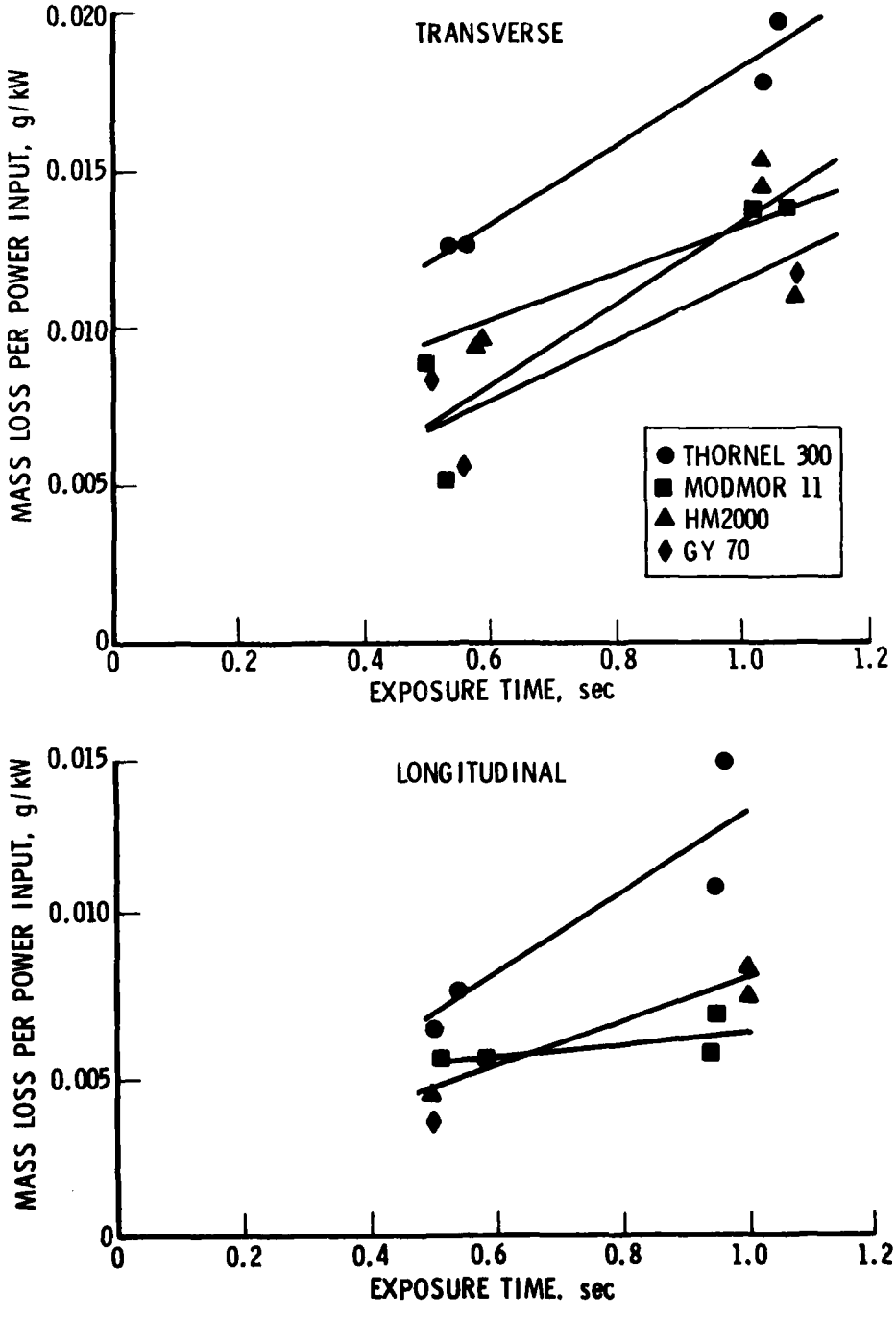

Figure 6. Mass Loss Data for PAN Precursor Filaments

Table 4. Linear Regression Analysis of Filament Mass Loss Data

System	Direction	Slope, 10^{-3} g kW^{-1} sec^{-1}	Y-Intercept, 10^{-3} g kW^{-1}	Correlation Coefficient	Y at t 1.0, 10^{-3} g kW^{-1}
WYB	Transverse	14.2	4.1	0.98	18.3
Thornel 50		13.8	0.8	0.98	14.6
Thornel 75		12.6	-1.6	0.91	11.0
Thornel 300		12.3	5.8	0.98	18.1
Modmor II		12.8	0.4	0.91	13.2
HM 2000		7.2	5.9	0.75	13.1
GY 70		9.5	2.0	0.87	11.5
Thornel P		10.6	3.8	0.99	14.4
WYB	Longitudinal	–	–	–	
Thornel 50		–	–	–	
Thornel 75		–	–	–	
Thornel 300		12.9	0.5	0.93	13.4
Modmor II		1.9	4.5	0.64	6.4
HM2000		6.9	1.2	0.98	8.1
GY 70		–	–	–	
Thornel P		5.6	2.6	0.99	8.2
PG	c	2.0	0.1	0.88	2.1
	a	2.0	-0.4	0.93	1.6
Low Pressure Pitch	–	0	5.5	1.0	5.5
High Pressure Pitch	–	4.2	0.5	1.0	5.0

Only two data points

Table 5. Filament Volume Fraction and Density for All Specimens

Specimen	System	Volume Fraction, %	Effective Density, g/cc
28	WYB	64	0.84
29		73	0.96
30		66	0.87
31		64	0.84
		67*	0.88*
5	Thornel 50	64	1.06
6		70	1.16
7		72	1.20
8		68	1.13
		69*	1.14*
17	Thornel 75	58	1.04
18		51	0.92
19		57	1.03
20		58	1.04
		56*	1.01*
9	Thornel 300	73	1.24
10		73	1.24
11		74	1.26
12		75	1.28
		74*	1.26*
13	Modmor II	71	1.21
14		75	1.28
15		76	1.30
16		76	1.30
		75*	1.27*
1	HM2000	68	1.23
2		65	1.18
3		66	1.19
4		68	1.23
33		64	1.16
		66*	1.20*
21	GY 70	57	1.12
22		67	1.31
23		65	1.27
		63*	1.23*
24	Thornel P	60	1.15
25		61	1.17
26		64	1.23
27		69	1.32
		63.5*	1.22*

*Average

Since the effective densities of the filament specimens varied slightly, the mass loss data were also analyzed in terms of volume loss per unit of power. Volume loss was calculated by dividing mass loss by filament density. A linear regression analysis of the volume loss data revealed that the average correlation factors were 0.93 and 0.92 for the volume loss and mass loss, respectively. With such similar results, it was decided to present the data in terms of mass loss.

The pyrolytic graphite was expected to have very low mass loss values. The values were a factor of four to nine times lower than those for the filaments, with the a-direction being 31 percent greater than the c-direction (see Figure 7). The bulk matrix coal tar pitch specimens had remarkably low values, slightly lower than the longitudinal direction of the filaments (see Figure 8). Unfortunately, only a limited number of composites could be irradiated. The three composites that were tested (see Figure 8) had mass loss values equivalent to pyrolytic graphite (see Figure 7). Although the composites could be ranked in terms of mass loss rate, the average mass loss rates were very close, being 0.0134 g/kW for composites processed by low pressure procedures, 0.0199 g/kW for mixed pressure processing, and 0.0216 g/kW for high pressure processing.

B. MICROSCOPY

The appearances of the craters in all filament specimens were similar and of a triangular shape except for the Thornel 300 filament (see Figures 9 through 11). The slightly larger craters in the transverse specimens reflected the greater mass loss of the transverse direction. The crater in the longitudinal direction of the Thornel 300 filament was significantly different from those in the other materials in that the filaments splayed out from the crater (see Figure 10a). The WYB and Modmor II filaments had a small amount of splay from the longitudinal crater. With a slight increase in magnification, additional details of the craters are evident (see Figures 12 and 13). The small amount of filament splay present in the

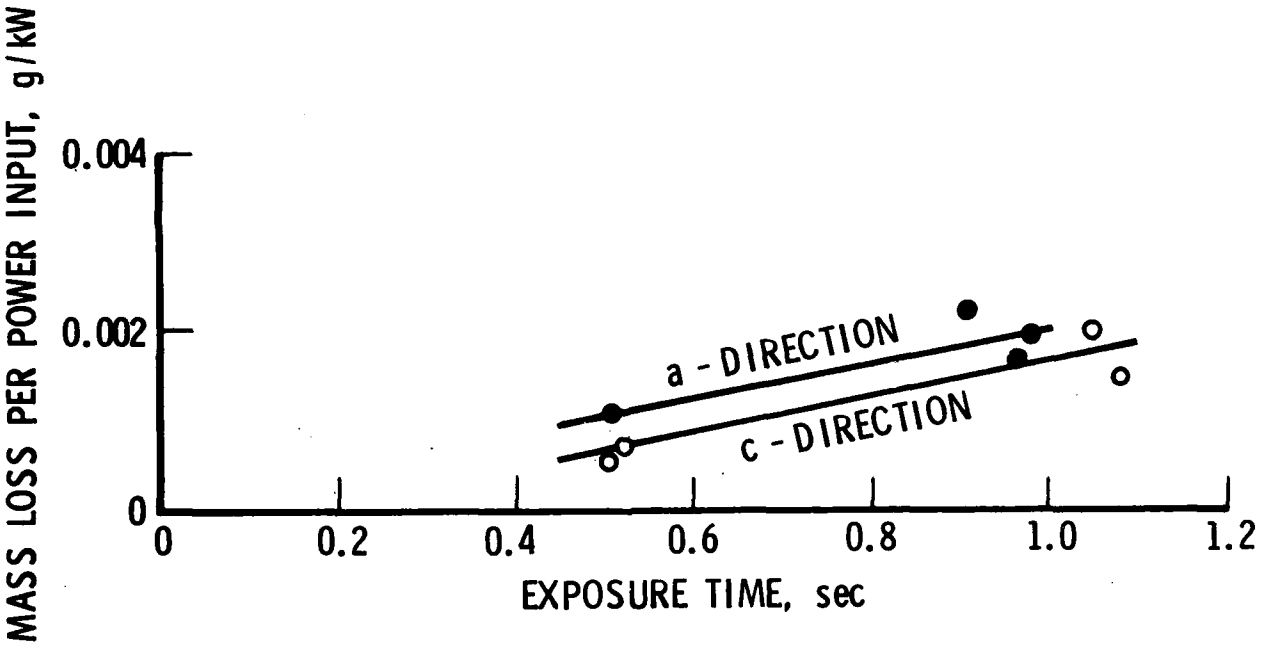

Figure 7. A- and C-Direction Mass Loss for Pyrolytic Graphite

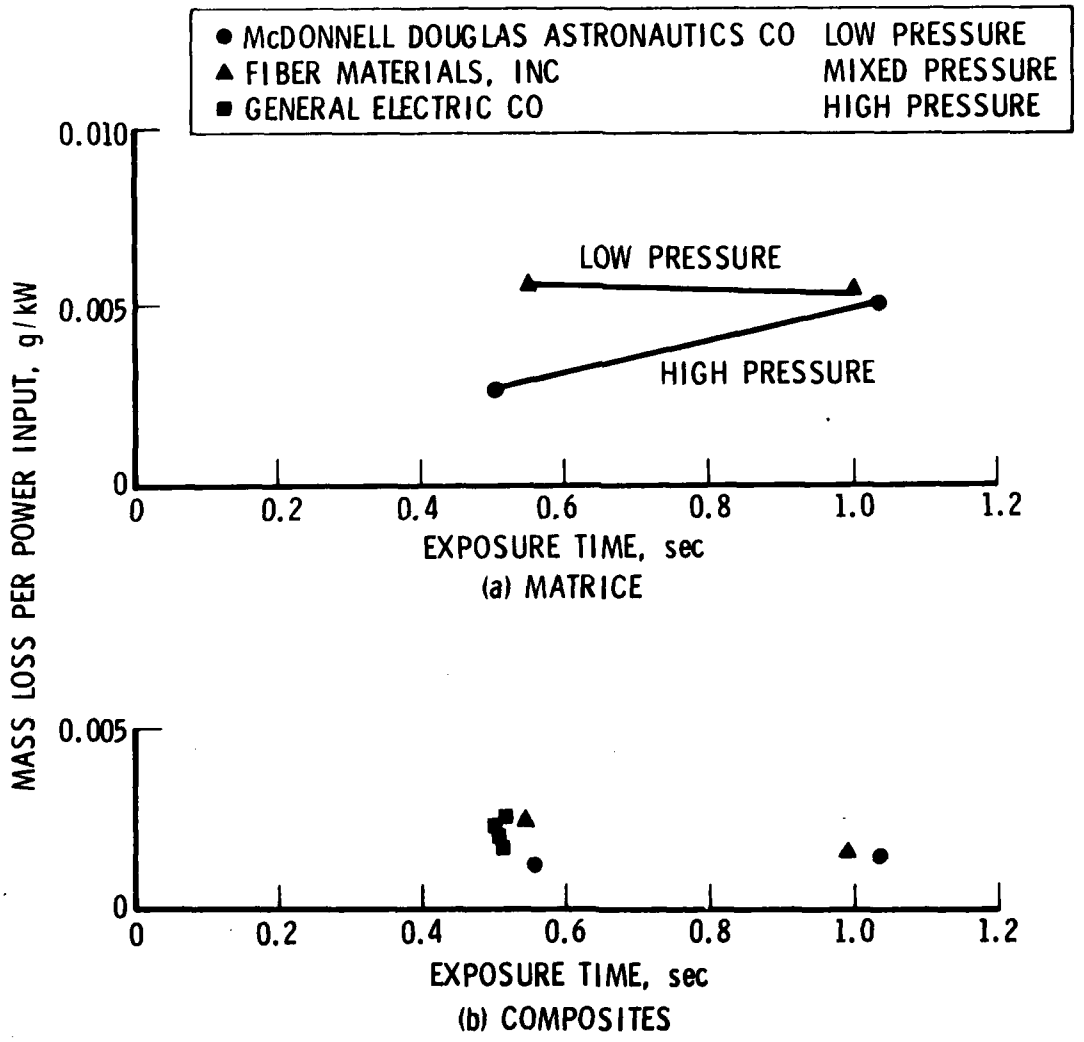

Figure 8. Mass Loss Data for Pitch Matrix (a) and Carbon-Carbon Composites (b)

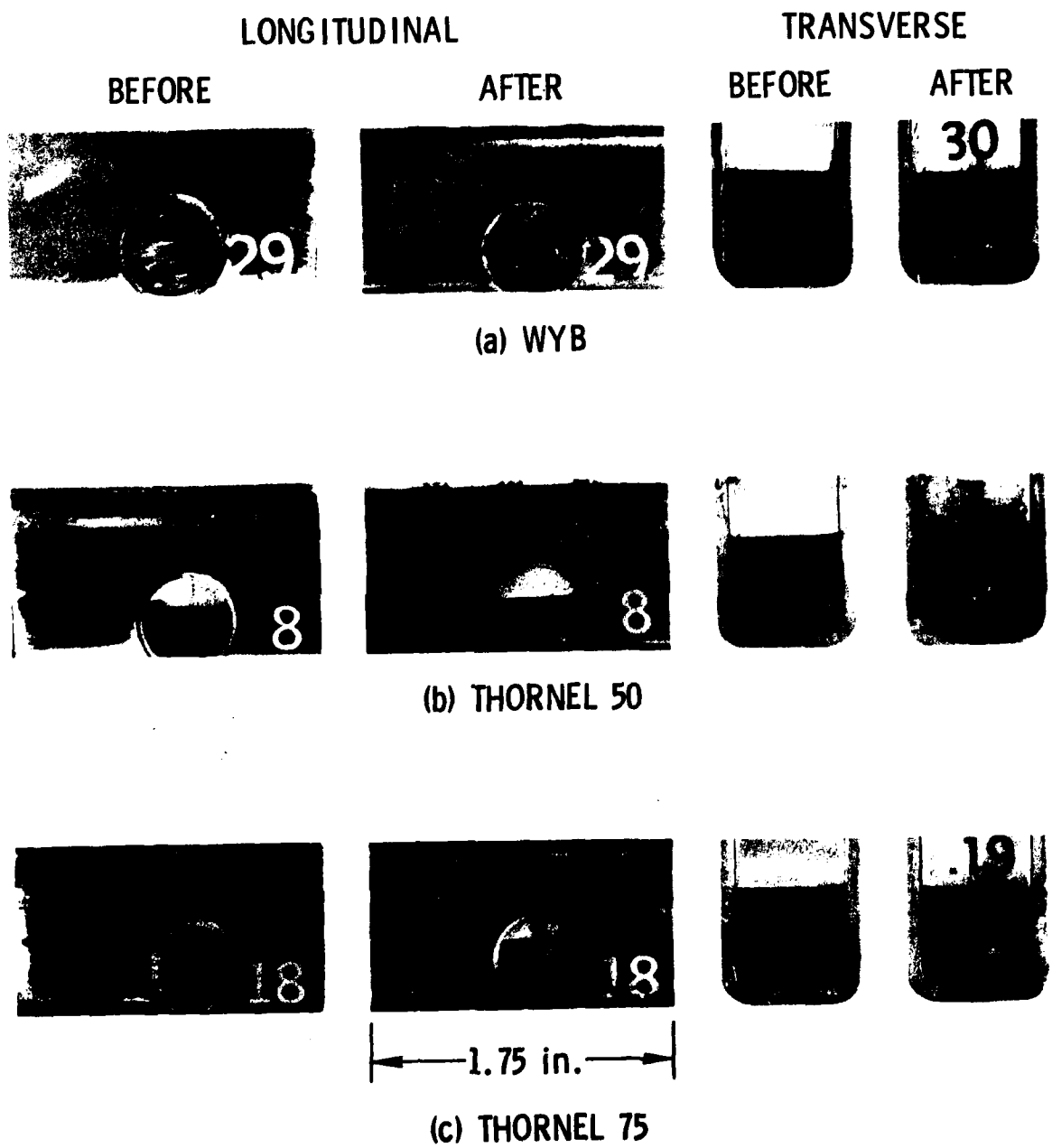

Figure 9. Optical Macrographs of Rayon Precursor Filaments Before and After Laser Irradiation

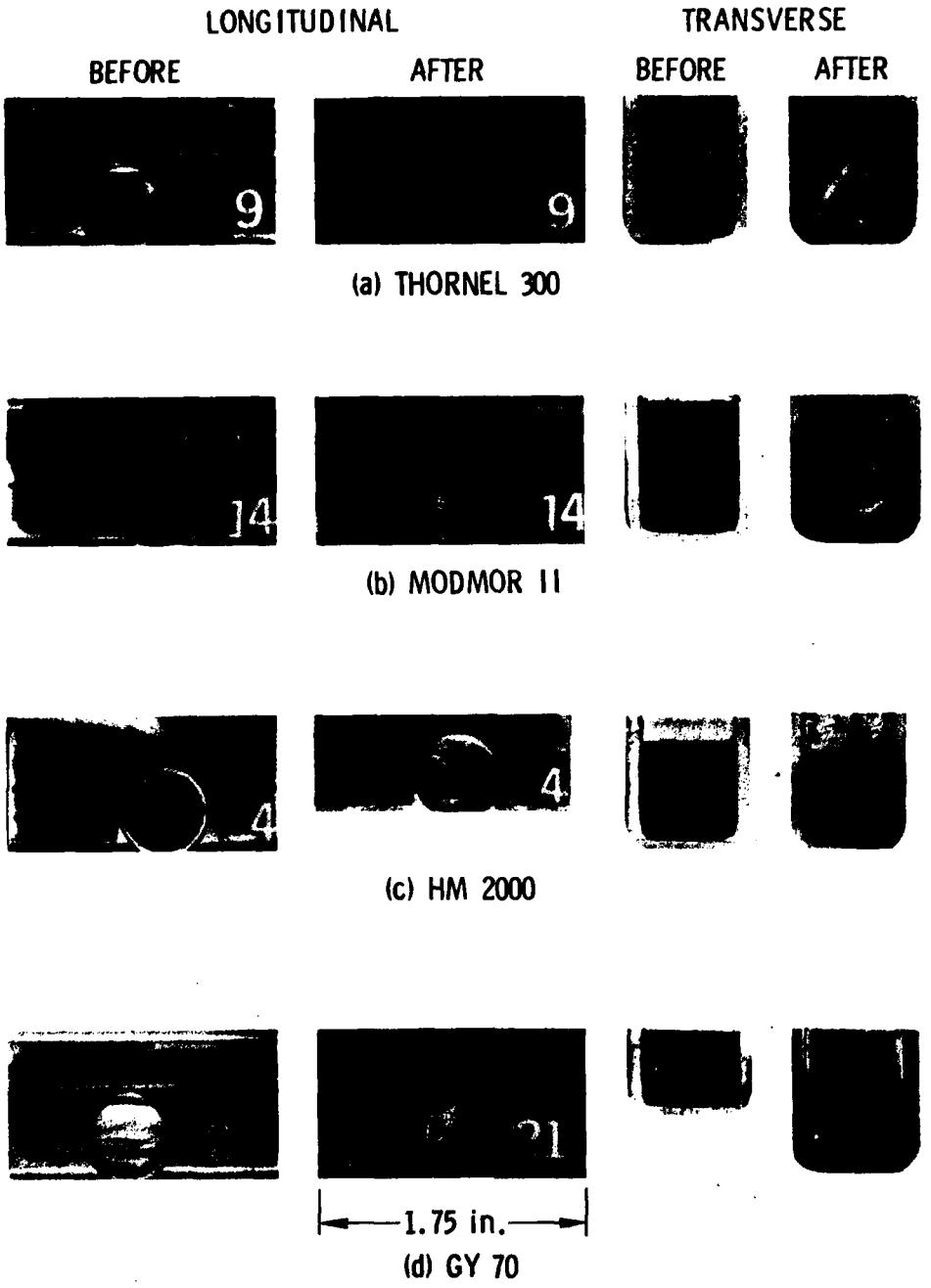

Figure 10. Optical Macrographs of Polyacrylonitrile Precursor Filaments Before and After Laser Irradiation

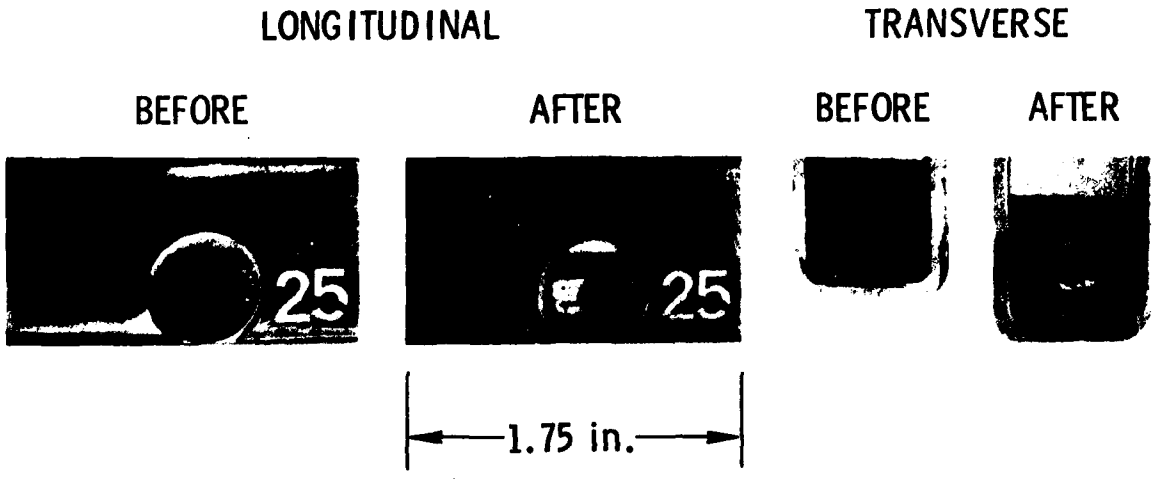

Figure 11. Optical Macrographs of Petroleum Pitch Precursor Filament Before and After Laser Irradiation

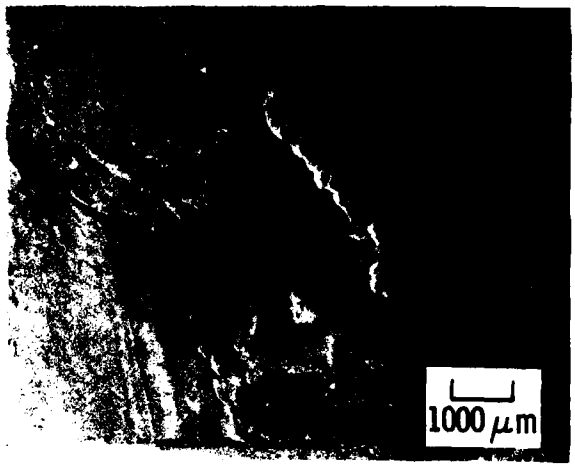

THORNEL 50

THORNEL P

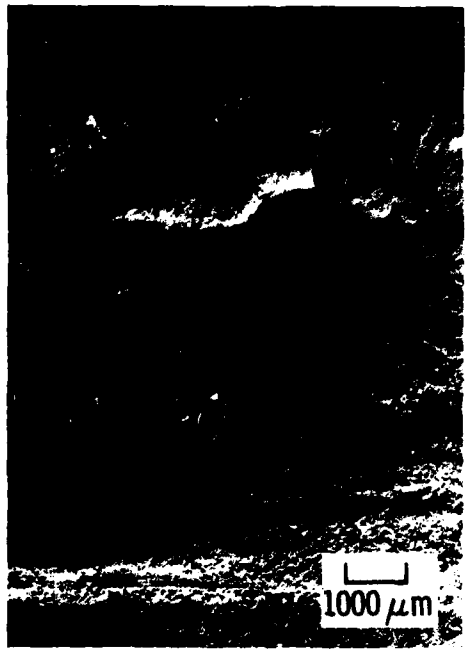

HM 2000

Figure 12. Scanning Electron Micrographs of Transverse Filament Craters

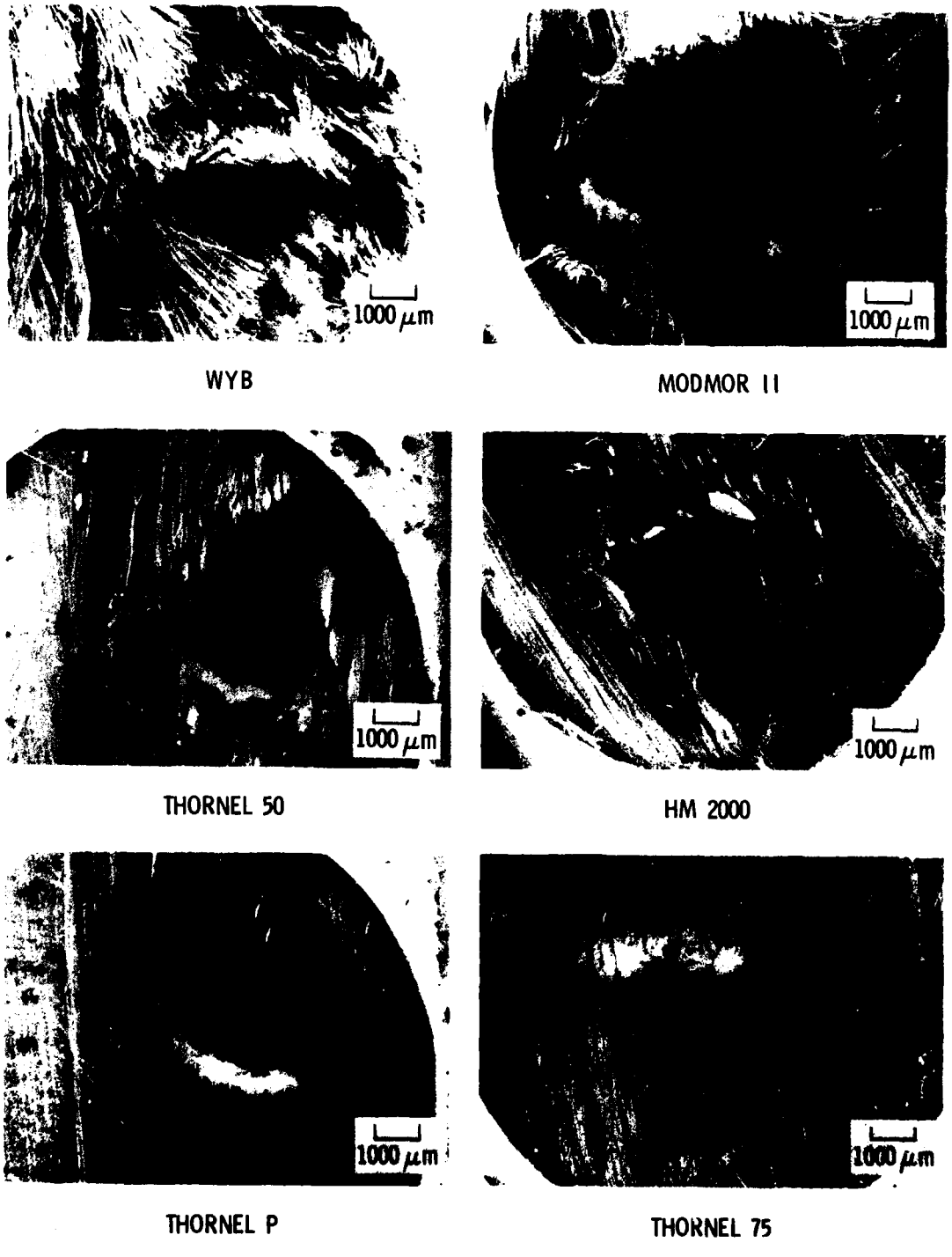

Figure 13. Scanning Electron Micrographs of Longitudinal Filament Craters Showing Filament Splay

longitudinal specimens is apparent. The coating on and in the craters is re-deposited carbon which occurred during cooldown.

Craters in the bulk pitch are shown in Figure 14. In general, the characteristics of these craters were not unusual. Some additional information on pore structure and orientation was obtained at a higher magnification of the HiPIC (high pressure) sample. The distribution of closed pores in this high pressure sample is quite evident (see Figure 15).

Craters in the multidirectional composites were very small in comparison to those in the filaments due to the significantly higher density and heat capacity of the composites (see Figure 16). The composite specimens were sectioned to view the point of maximum penetration. The specimens were not divided through the maximum diameter of the crater to form the sections, so the diameter of the crater must be taken from the top view and not from the cross-sectional view. Figures 17 through 20 show the top and side views of the craters in the composites processed by high (D2-2 and B1-2) and low (AX-1) pressure pyrolysis procedures. The smaller craters in the composites processed by low pressure procedures were surprising. The craters in D2-2 and B1-2 were approximately eight times deeper than those in AX-1. Although AX-1 had a more shallow crater, it encompassed a larger area. This is in comparison to the deeper but narrower crater in the samples processed by high pressure procedures. Again, these observations are consistent with the high mass loss (60 percent) of the composites processed by high pressure.

The pyrolytic graphite control samples had the expected small craters, particularly in the a-b face (see Figure 21). The crater on the c-face was elongated in the direction of higher thermal conductivity (see Figure 22). Examination of the crater on the a-b face at a higher magnification did not reveal additional information (see Figure 23).

1.0 in.

(a) 1,000 psi PYROLYSIS PRESSURE

(b) 15,000 psi PYROLYSIS PRESSURE (HIPIC)

Figure 14. Optical Micrographs of Coal Tar Pitch Precursor After Laser Irradiation

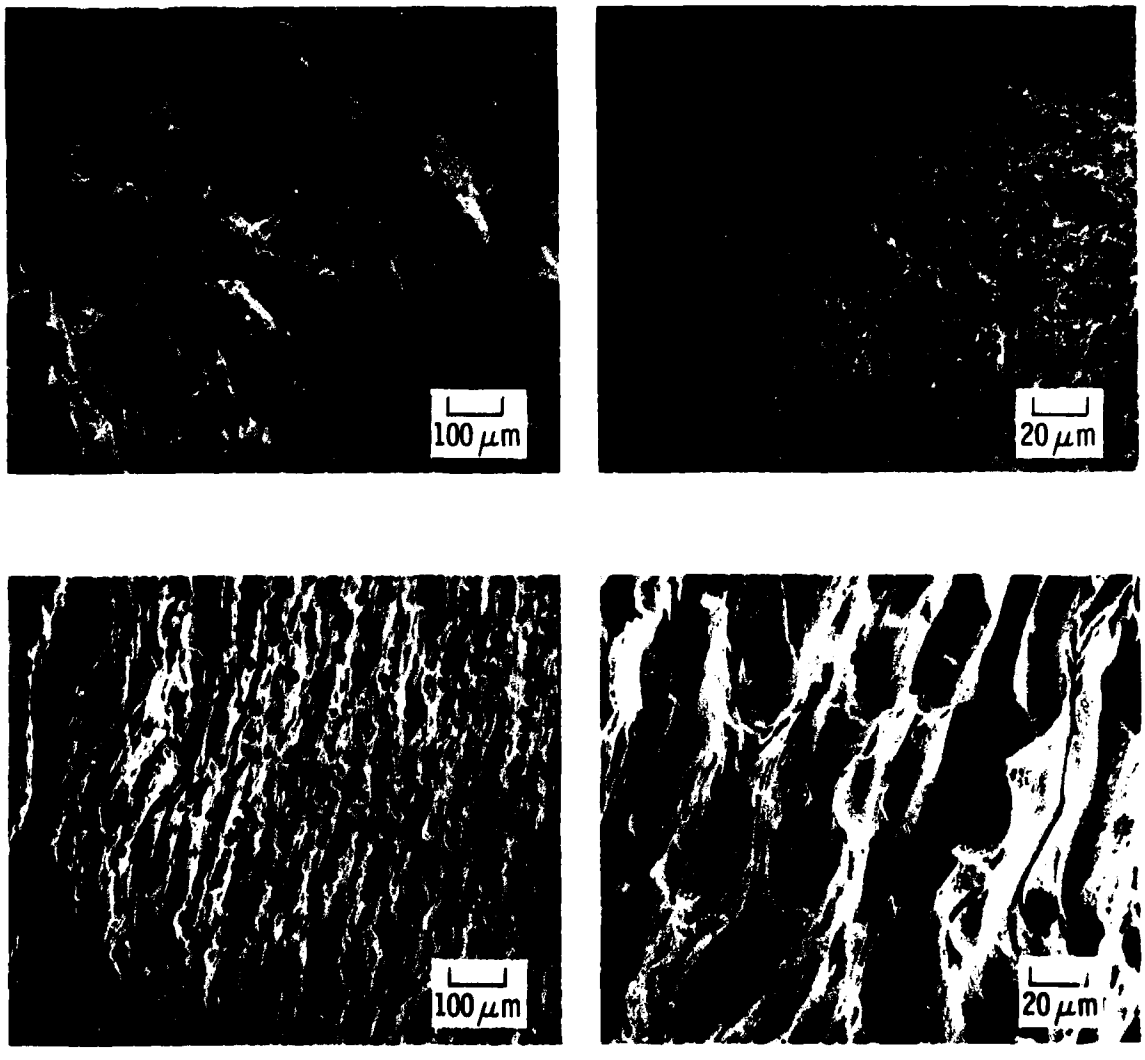

Figure 15. Scanning Electron Micrographs of Bulk Matrix Pyrolyzed by HiPIC Procedure (-1)

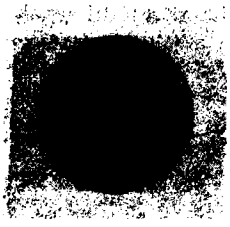

(a) 1,000 psi PRESSURE PYROLYSIS
COMPOSITE AX-2

(b) CVD + 15,000 psi PYROLYSIS
PRESSURE COMPOSITE D2-1

Figure 16. Optical Micrographs of Multi-Directional Composites After Laser Irradiation

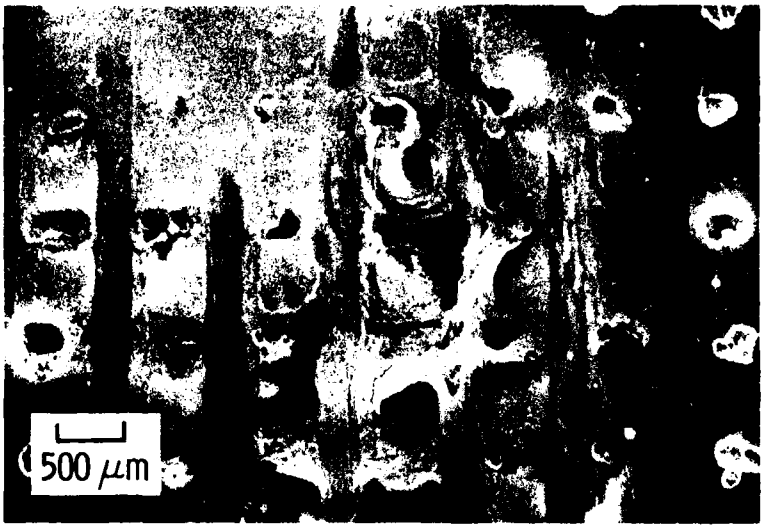

TOP VIEW

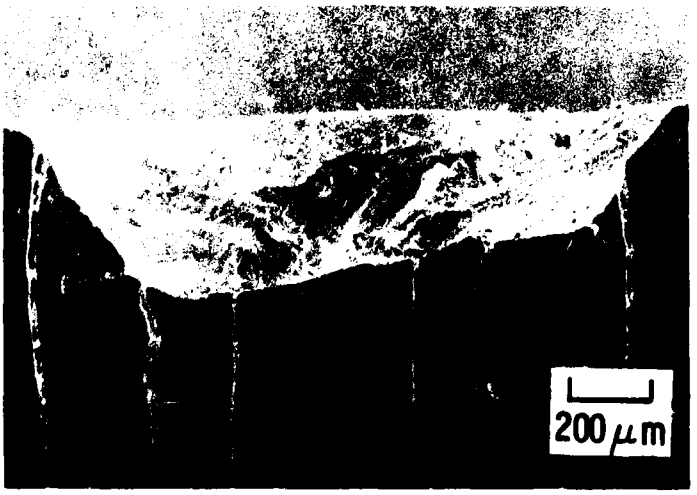

SIDE VIEW

Figure 17. Scanning Electron Micrograph Top and Side Views of AX-1 Crater

Figure 18. Scanning Electron Micrograph Top View of D2-2 Crater

Figure 19. Scanning Electron Micrograph Side View of D2-2 Crater

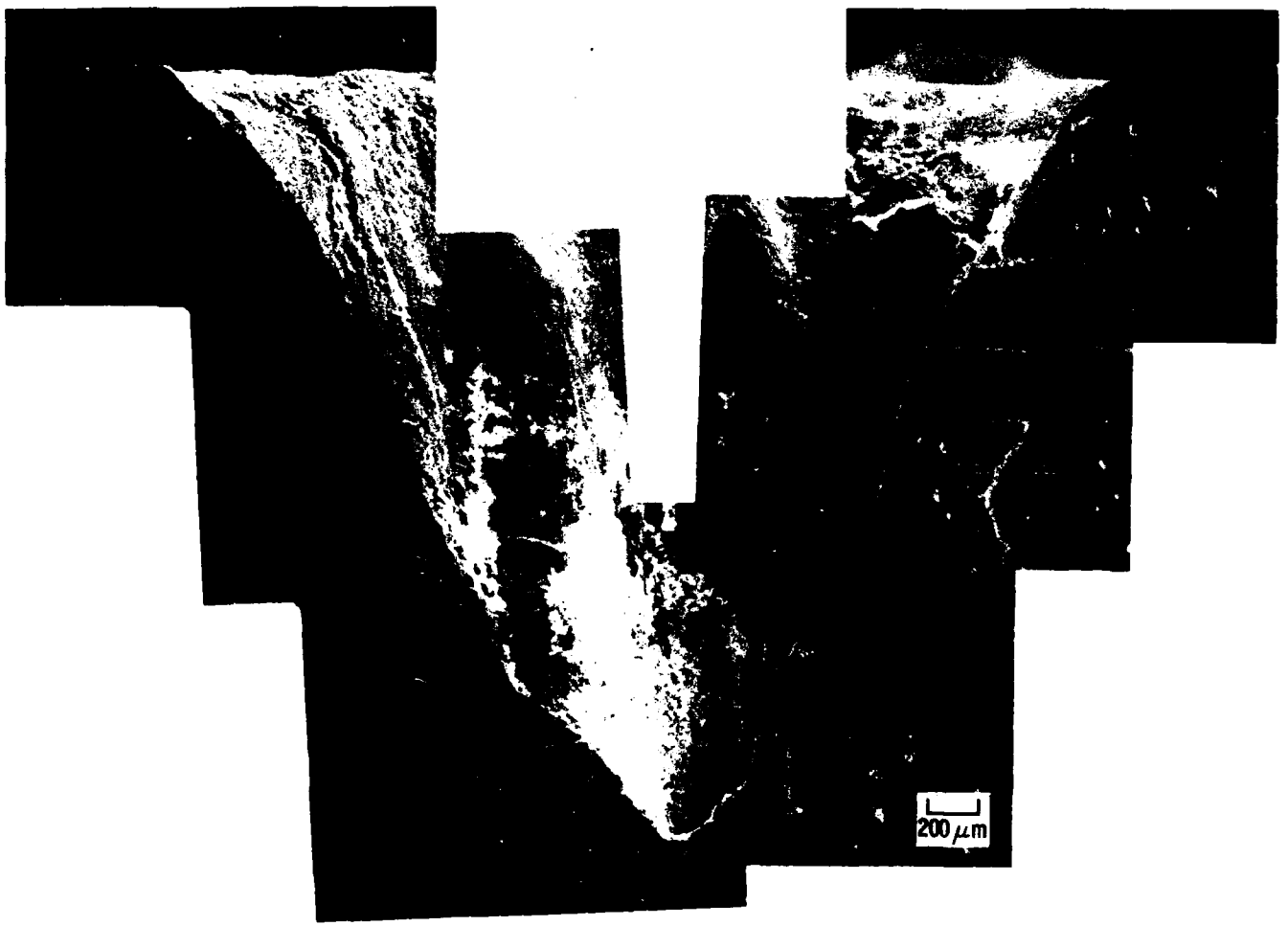

Figure 20. Scanning Electron Micrograph Side View of B1-2 Crater

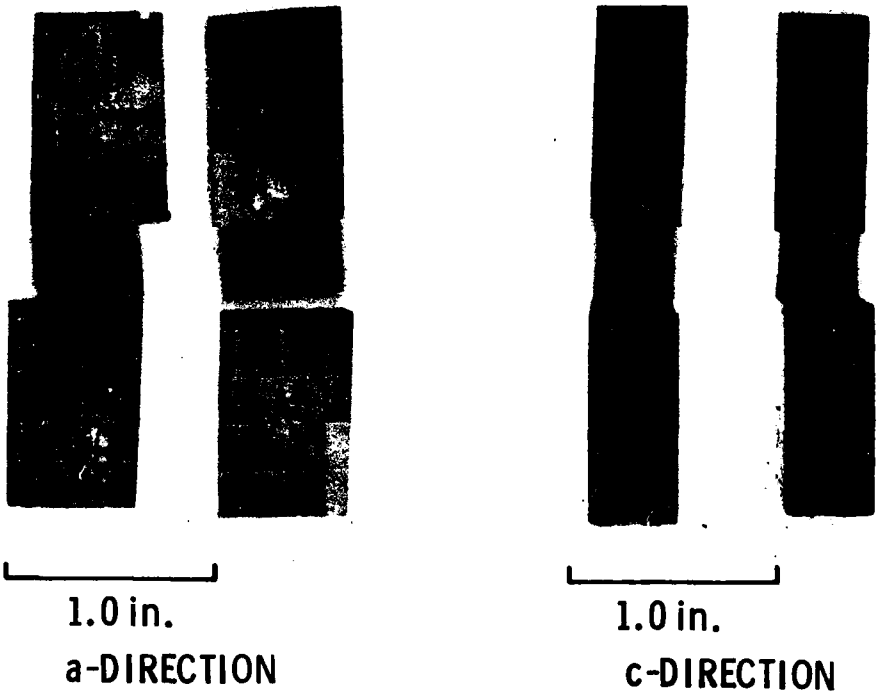

Figure 21. Optical Macrographs of Pyrolytic Graphite After Laser Irradiation

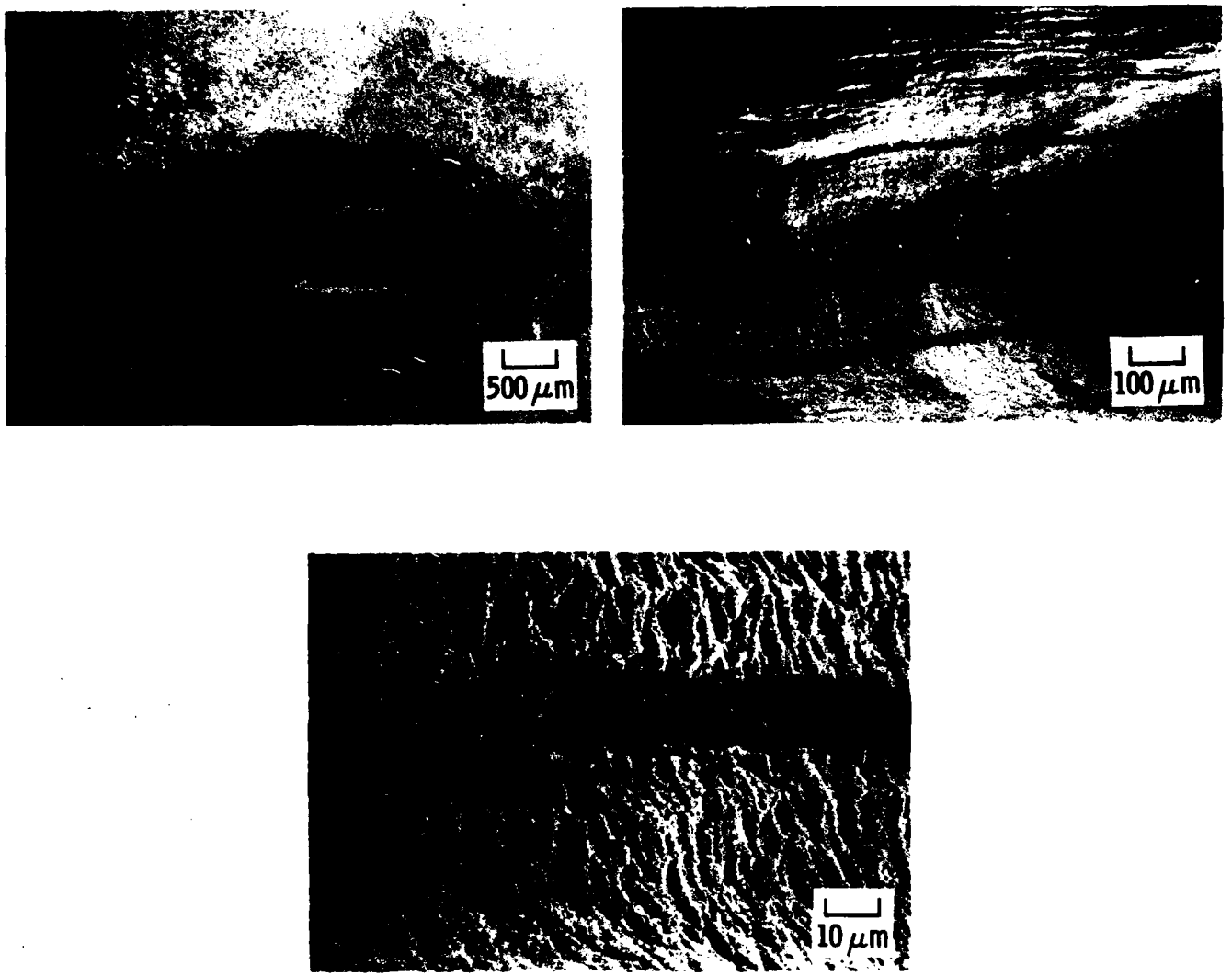

Figure 22. Scanning Electron Micrographs of a Crater in Pyrolytic Graphite Control Sample No. 1 in C Plane

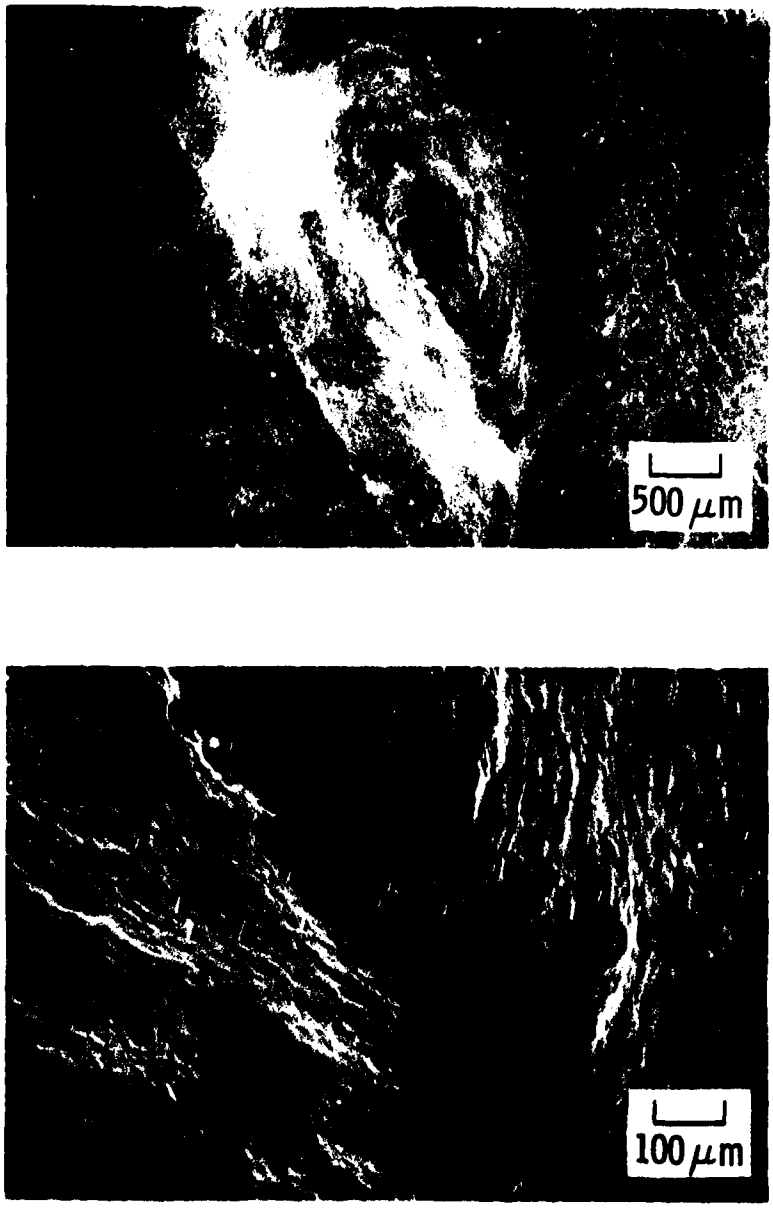

Figure 23. Scanning Electron Micrographs of a Crater in Pyrolytic Graphite Control Sample No. 1 on A-B Plane

V. DISCUSSION

In the laser irradiation experiment, several of the relationships which were believed to exist between filament mass loss and filament orientation, modulus, and density were examined. The equations from the linear regression analysis were used to calculate mass losses for each system after a one-second irradiation (see Figure 24). The three filaments of interest to the aerospace community, Thornel 50, HM2000, and Thornel P, had equivalent responses in both directions. The bar chart suggests possible correlations of mass loss rate with density, modulus, or the product of modulus and density. These are shown in Figures 25 thru 27 and the regression analysis results are tabulated in Table 6. Good correlations were found for modulus and the product of modulus and density with a reasonable correlation found for density alone. Incorporating the pyrolytic graphite data into the correlation (density of 2.15 g/cc and a modulus of 100) resulted in equally good correlations (see Table 6).

The results confirmed the importance of physical and mechanical properties in controlling mass loss, and also revealed that one single property cannot determine mass loss. This is illustrated by a comparison of Thornel 50, HM2000, and Thornel P filaments which had equivalent mass losses, but which were of differing precursors (rayon, PAN, and pitch, respectively), differing densities (1.66, 1.81, and 1.92 g/cc, respectively), but similar moduli. A second example is a comparison of Thornel 300 and Modmor II, which had different mass losses while having equivalent densities and moduli. However, their precursors are not of the same PAN family. Another comparison is between WYB, Thornel 50, and Thornel 75. All are from a similar precursor, yet each differs in density and modulus, further supporting the importance of these two properties. Modulus is a result of crystallographic orientation; consequently, the degree of graphitic registry and the arrangement of these crystallites into macrostructural units are both important structural parameters.

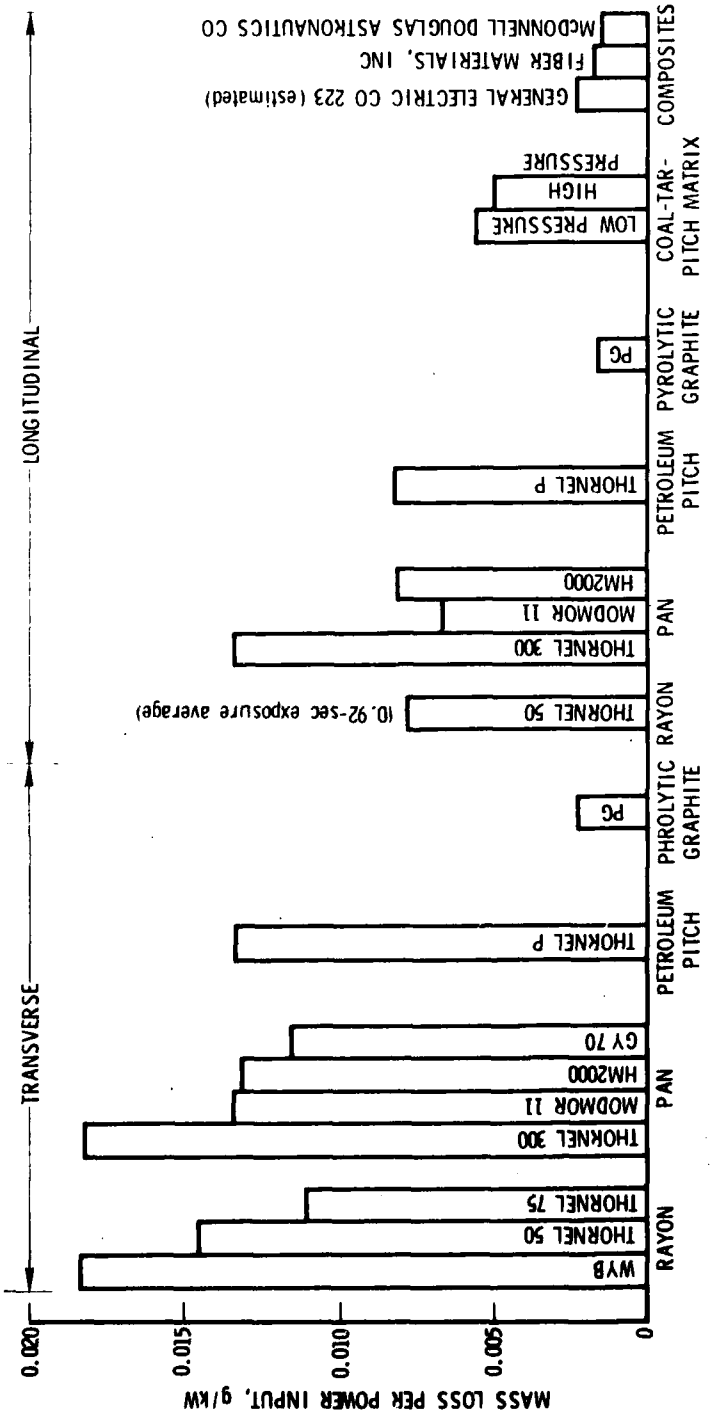

Figure 24. Mass Losses from Linear Regression Analysis for a One-Second Irradiation

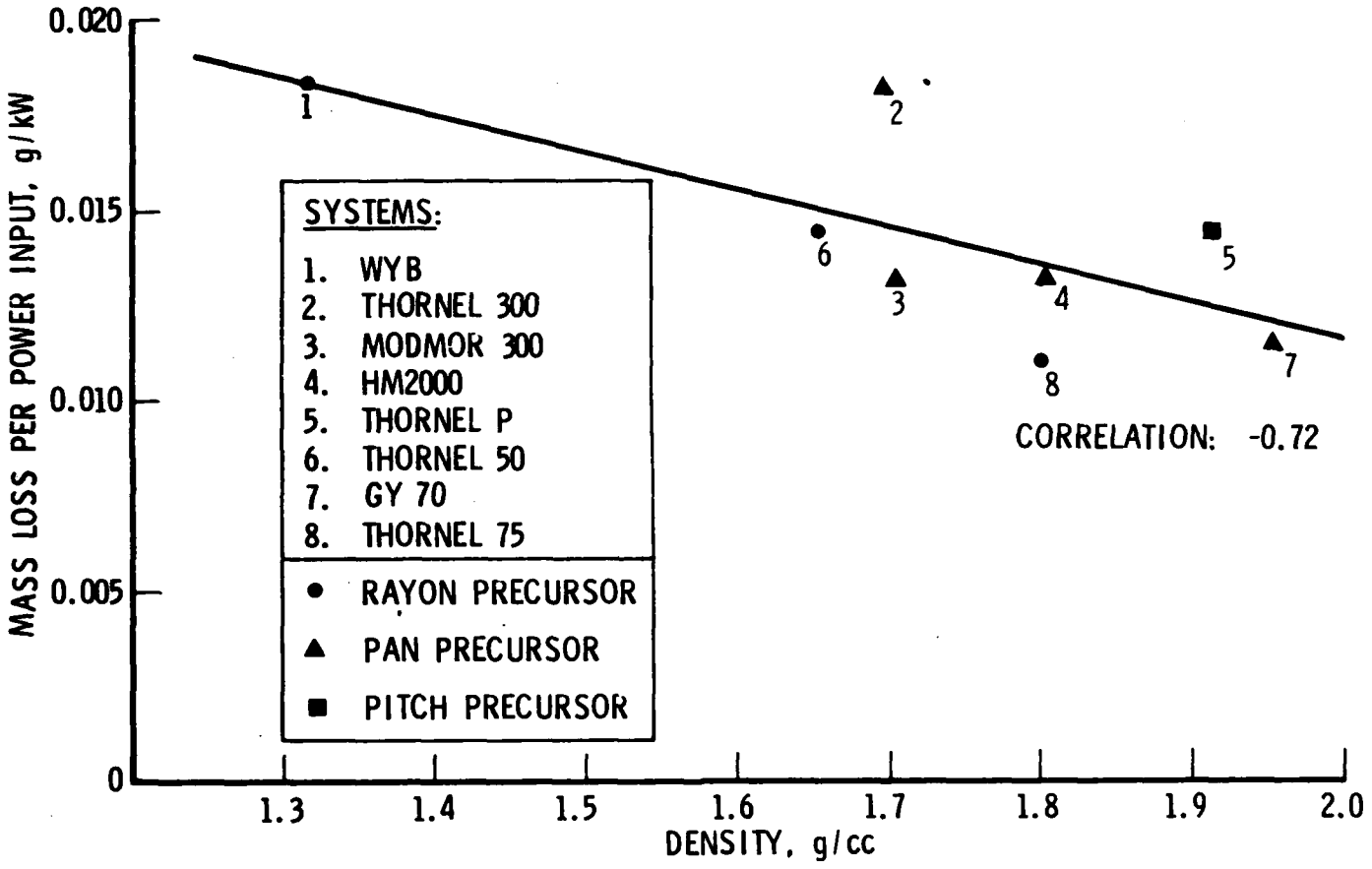

Figure 25. Mass Loss in Transverse Direction Per Power Input versus Filament Density

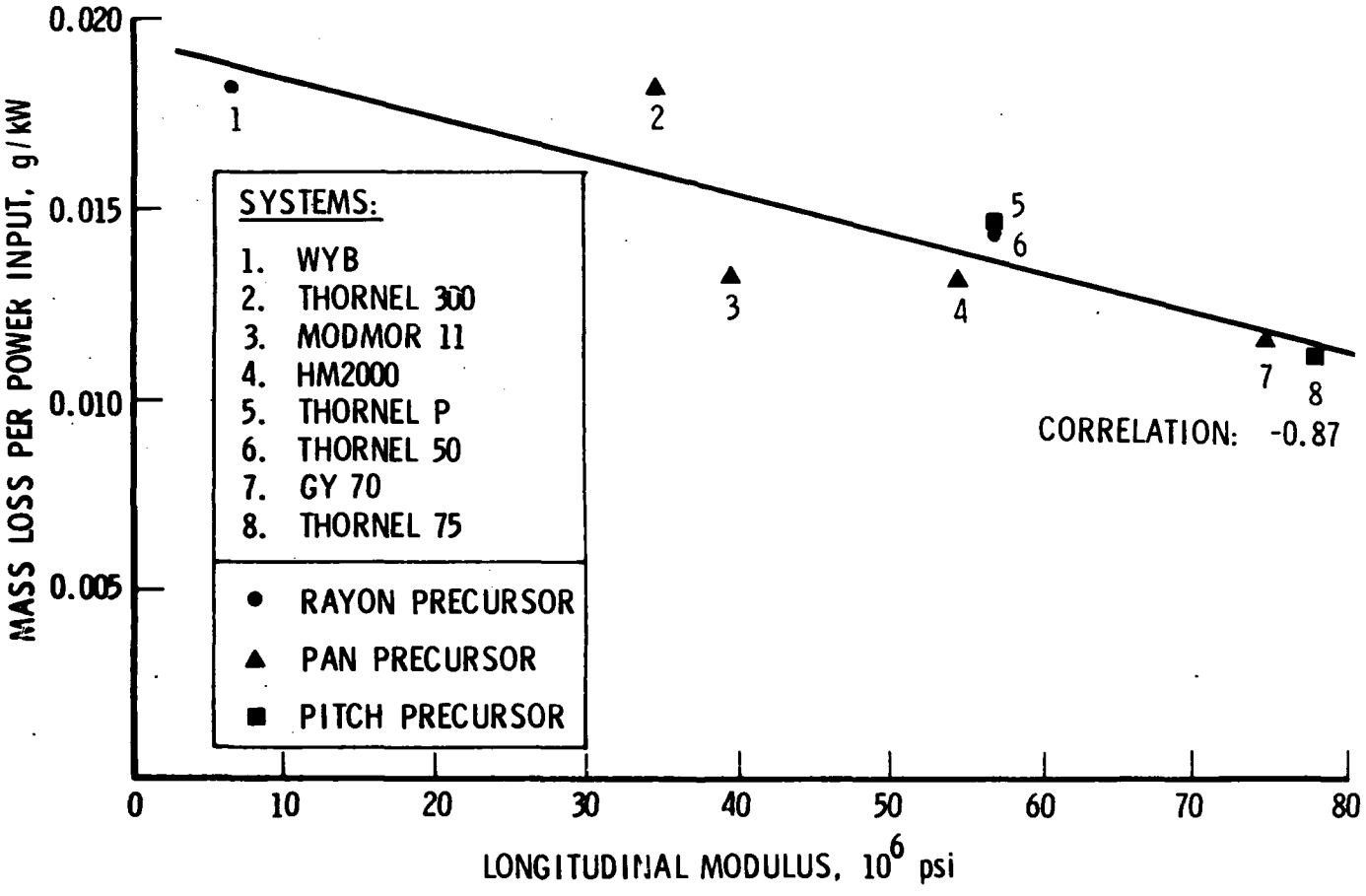

Figure 26. Mass Loss in Transverse Direction Per Power Input versus Filament Longitudinal Modulus

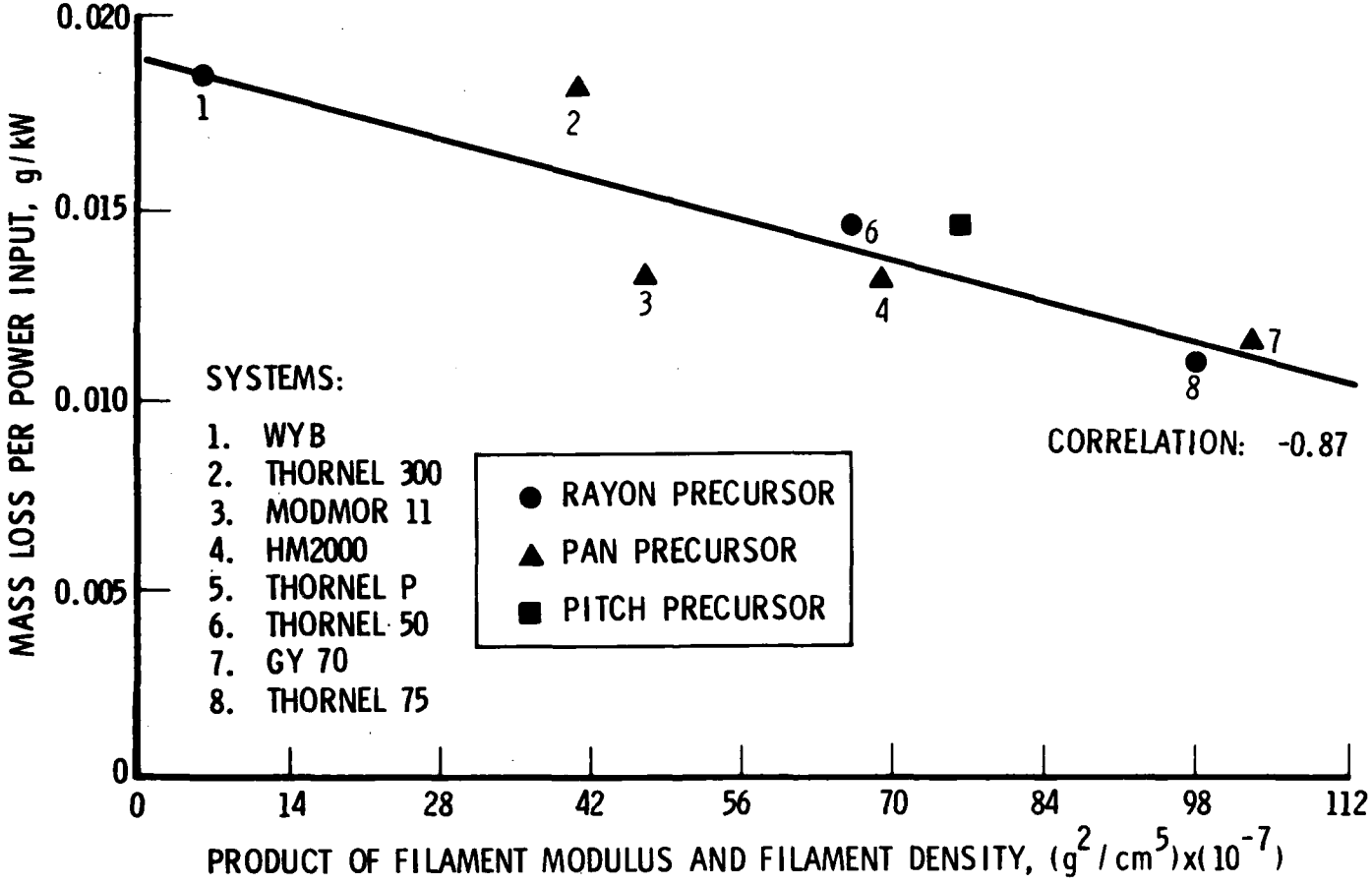

Figure 27. Mass Loss Per Power Input versus the Product of Filament Modulus and Density

Table 6. Linear Regression Analysis of Filament Mass Loss Property Relationships

Without Pyrolytic Graphite Data			
Property	Correlation Coefficient	Slope, cc/kW	Y-Intercept, g/kW
Density	-0.72	-.0099	.0314
Modulus	-0.87	-.0010	.0193
Density & Modulus	-0.87	-.0005	.0190
Using Pyrolytic Graphite Data			
Property	Correlation Coefficient	Slope, cc/kW	Y-Intercept, g/kW
Density	-0.85	-.0184	.0467
Modulus	-0.88	-.0015	.0215
Density & Modulus	-0.96	-.0008	.0190

The mass loss data from the longitudinal filament orientation were similar, ranging from only 6.4 to 13.4 g/kW. If the 13.4 g/kW is omitted, the range was from 6.4 to 8.2 g/kW. The 13.4 value was for the Thornel 300 filament which had the large amount of filament splay from the crater (see Figure 10a). With such a dramatic crater, additional mass loss due to microfracturing resulting in a higher than normal mass loss might be expected. The similarity in mass losses in the longitudinal direction is not surprising considering the small 1.1 to 1.9 range in transverse moduli. In addition, there are some similarities in the microstructural characteristics, crystallite orientation, and structure as discussed in the following paragraphs.

Due to limited data on the bulk matrix and composite samples, only general comments can be made. The bulk matrix material eroded at a

slightly slower rate than the longitudinal filament orientation, while the transverse filament orientation eroded at the fastest rate. This ranking is similar to that observed in ablation testing of composite models.[8] The only difference is that the bulk matrix phase erodes at a slightly faster rate than the longitudinal filaments in actual testing. This reversed ranking of these two components may again be due to the large specimen size with higher heat capacity and therefore lower mass loss. The mass loss percentage was on the order of 0.3 percent as compared to 1.0 percent for the filaments.

The three composite specimens had similar low mass losses ranging from 0.6 percent to 0.1 percent. Longer exposure times at higher laser beam energies are needed to differentiate between these composites. However, the fact that they are equivalent is consistent with recession rates measured during ablation tests.[8] The low composite mass losses are due to two factors. First, approximately 80 percent of the composite consists of the low mass-loss constituents, i.e., longitudinal filaments and bulk matrix. Secondly, higher density and larger specimen size will result in lower mass losses.

The post-test analysis of the microstructural characteristics of individual filaments provided considerable information on filament response and structure of carbon filaments. Figure 28 shows the morphology structure and carbon filaments prior to irradiation. A summary of observations made from the scanning electron micrographs is tabulated in Table 7.

The rayon precursor filaments after irradiation are shown in Figures 29 thru 31. The rayon filaments typically eroded to a conical or slightly pointed shape. Internal flaws and microporosity can be found. The internal structure is most apparent in the WYB filament. Groups of oriented planes appear parallel to the surface of the filament, matching the filament crenulations.

---

[8] J. S. Evangelides, Presentation to the SAMSO Material Development Coordination Committee, El Segundo, CA (February 1977).

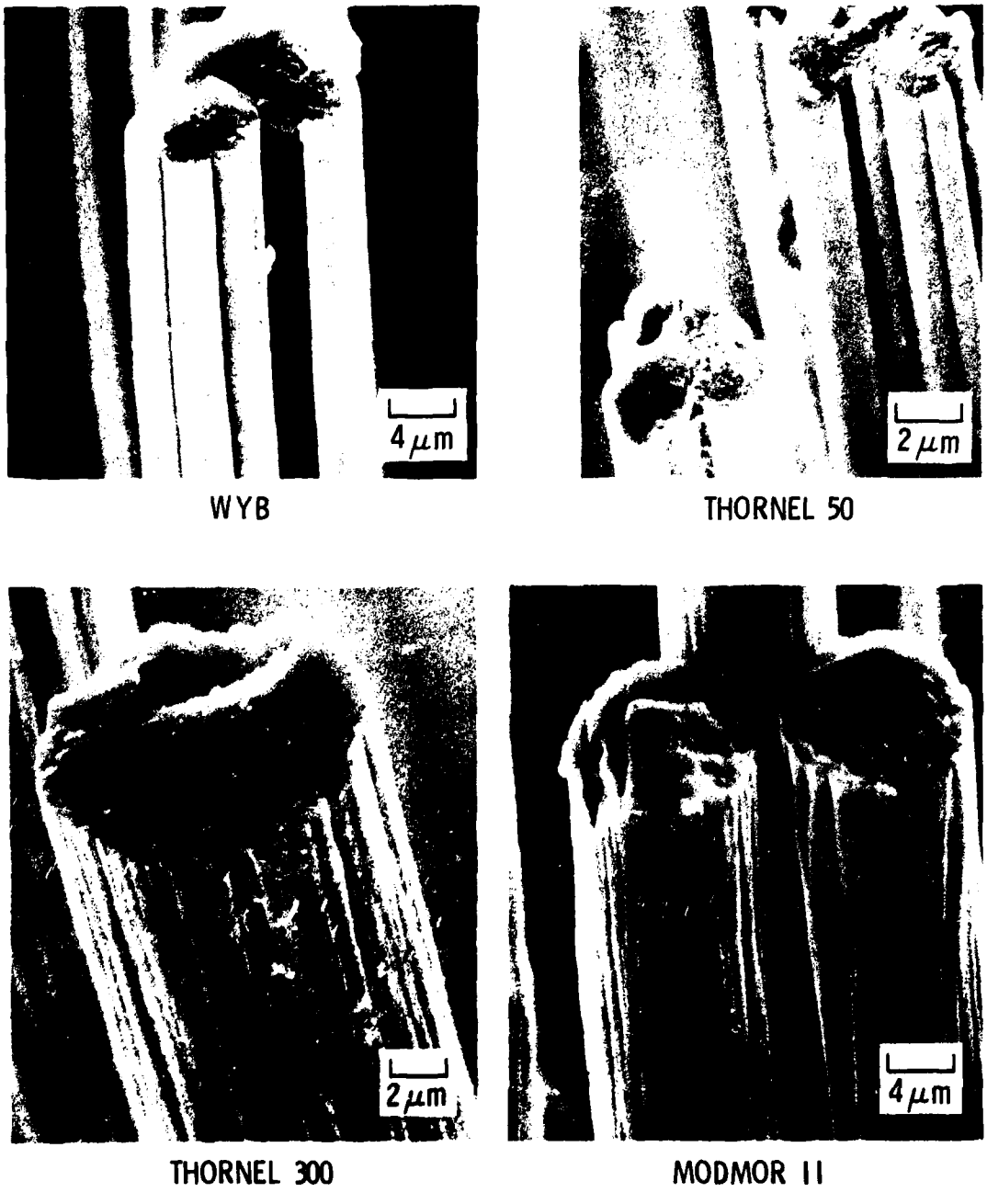

Figure 28(a). Scanning Electron Micrographs of Control Filaments Prior to Irradiation

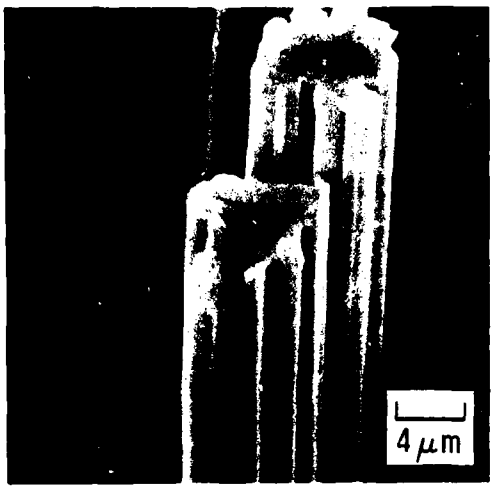

THORNEL 75

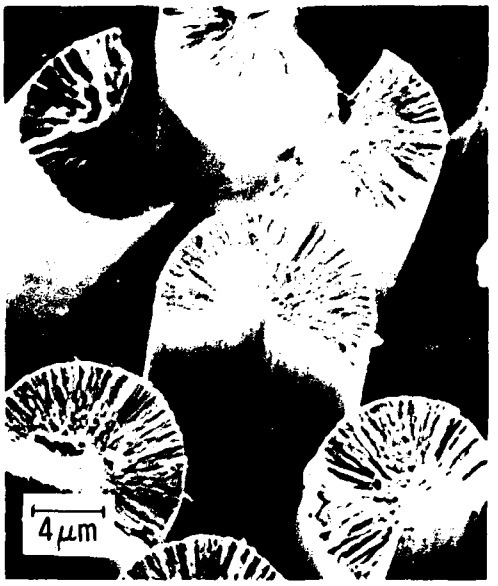

THORNEL P

HM 2000

GY 70

Figure 28(b). Scanning Electron Micrographs of Control Filaments Prior to Irradiation (Continued)

Table 7. Carbon Filament Characteristics from Scanning Electron Micrographs

Filament	Before Irradiation		After Irradiation	
	Shape	Internal Structure	Shape	Internal Structure
WYB	Crenulated	-*	Conical	Parallel to crenulations
Thornel 50	Crenulated	-*	Conical	Parallel to crenulations
Thornel 75	Crenulated	-*	Conical	Parallel to crenulations
Thornel 300	Cylindrical with striations	-*	Flat	Resistant sheath with less resistant core
Modmor II	Cylindrical with striations	-*	Conical-pointed	Circumferential (segmented)
HM2000	Cylindrical	-*	Conical-pointed or flat cone	Cylindrical ("onion skin")
GY 70	Dogbone	-*	Tapered-cone	Core occasionally less resistant
Thornel P	Cylindrical and pie-shaped with slight striations	Radial	Tapered	Radial

*Too small to be discerned.

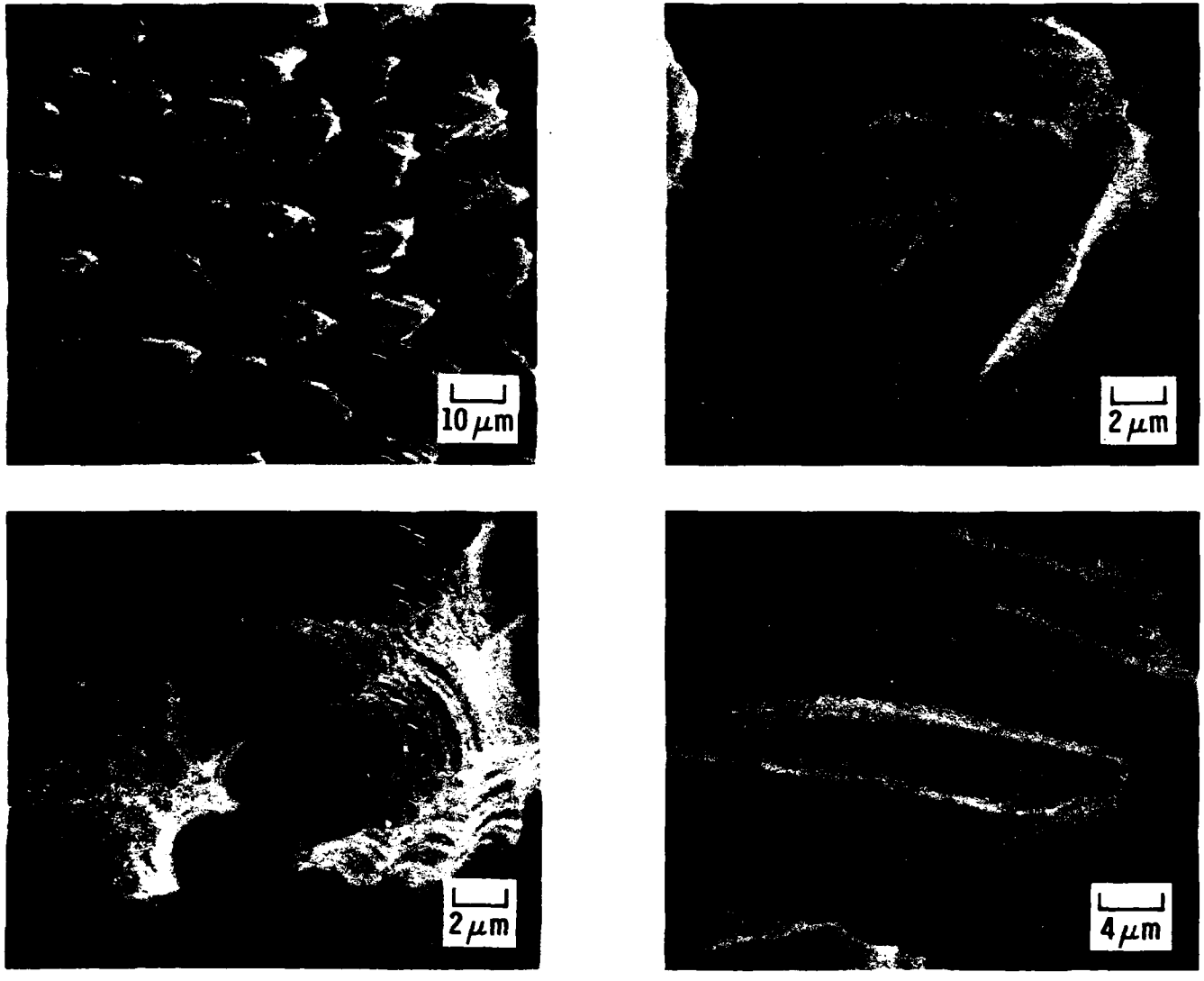

Figure 29. Scanning Electron Micrographs of WYB After Irradiation

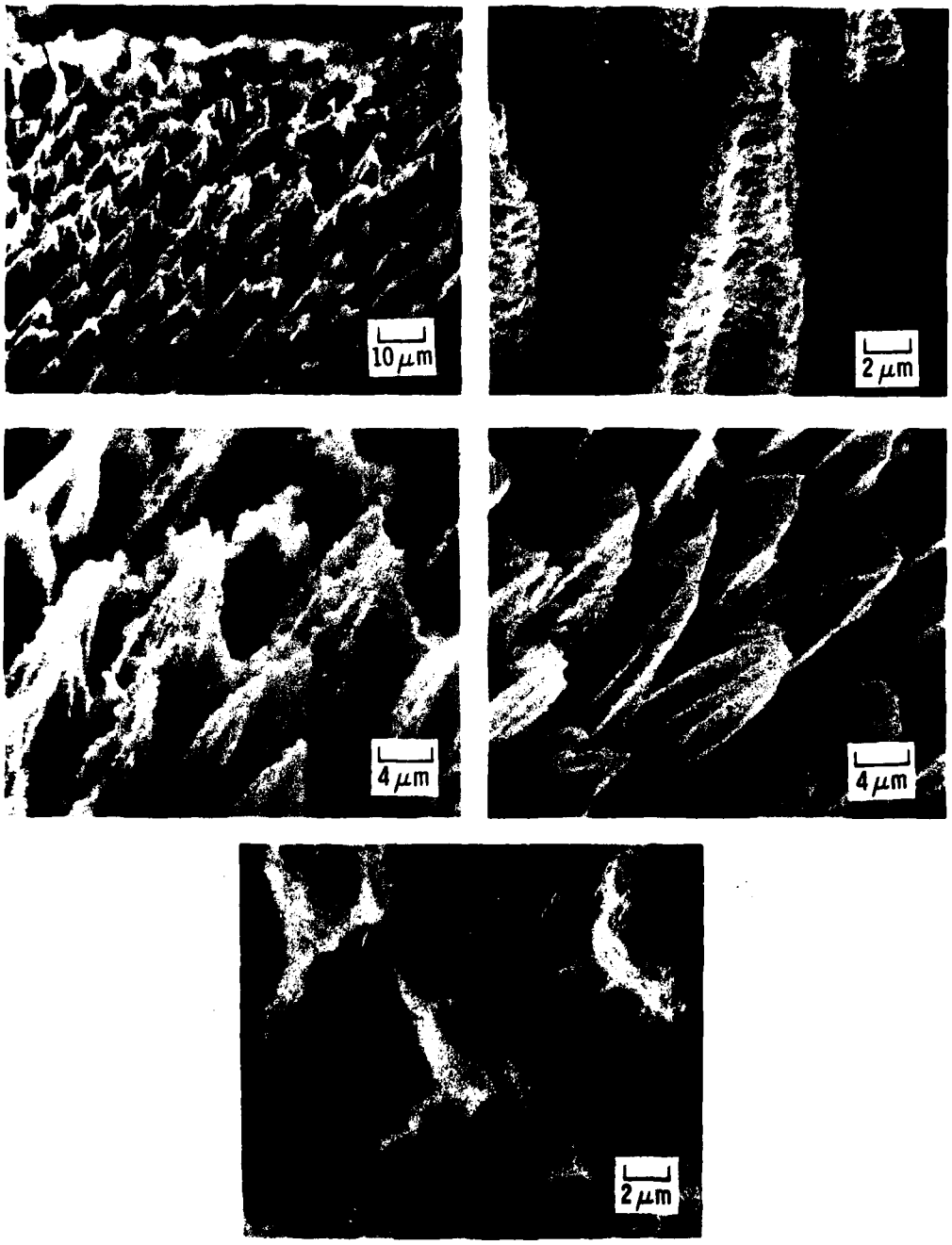

Figure 30. Scanning Electron Micrograph of Thornel 50 After Irradiation

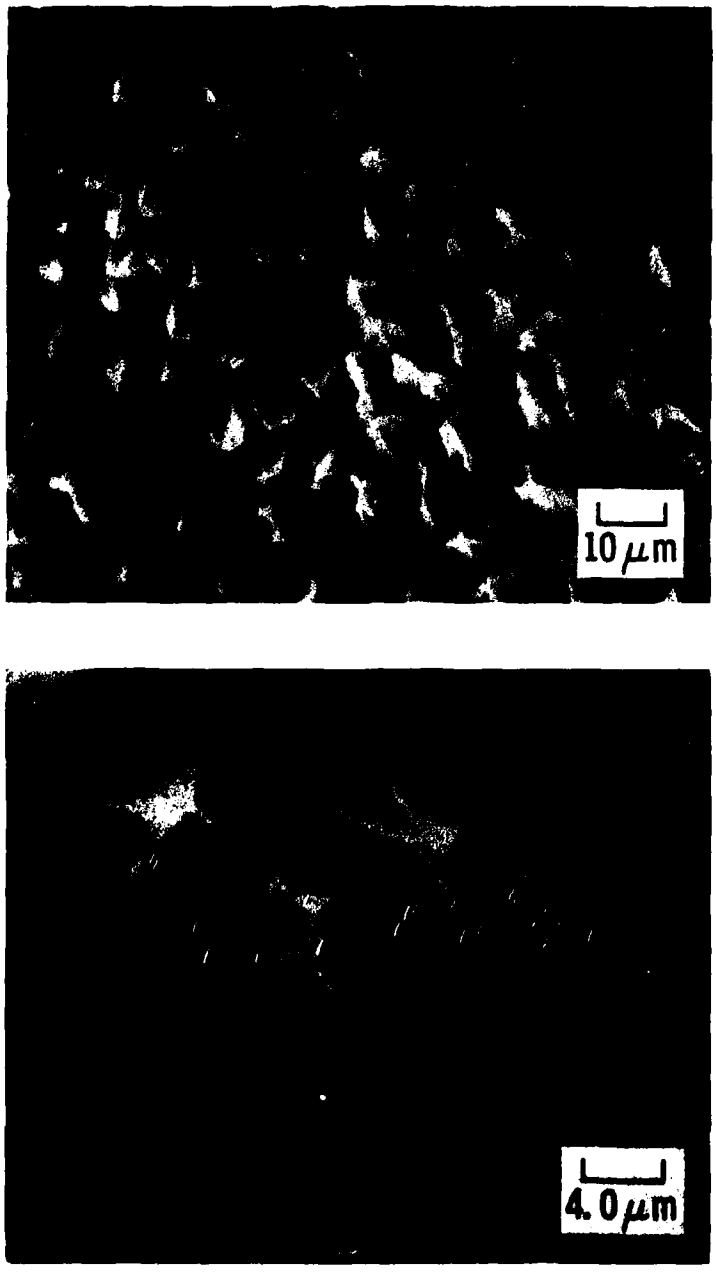

Figure 31. Scanning Electron Micrographs of Thornel 75 After Irradiation

The PAN precursor cross section filaments were cylindrical, with the exception of GY70, which was in the shape of a dog bone. After irradiation, each of the PAN filaments assumed a different characteristic shape (see Figures 32 thru 35). Thornel 300 had the most intriguing shape. An extremely thin sheath surrounded the filaments and was noticeably more erosion-resistant (see Figure 32). The filament center was the least resistant to ablation. This center region had either a very fine graphitic structure or a random structure. Filament segments or wedges radiated from the low center to the higher sheath. The ends of the Thornel 300 filament had the flattest post-test appearance. Modmor II assumed a conical shape with a circumferential structure which appeared segmented as shown in Figure 33. The HM2000 also assumed a conical shape, but with either a fine point or a flat ablation-resistant core. The HM2000 structure was uniform, with an "onion skin" or cylindrical orientation (see Figure 34). These results are similar to those obtained by Barnet and Norr.[9] The GY 70 filaments tapered at the ends with a wedge-like appearance (see Figure 35). Occasionally a center-core pore was present. The internal structure was difficult to discern in the GY 70 filament.

The final filament to be examined was the Thornel P filament which was tapered, with the core being the least ablation-resistant (see Figure 36). The radial structure extending to the surface was still apparent. A brief comparison of the filament microstructure after irradiation for the filaments of interest is shown in Figure 37. This should be compared with Figure 38 which shows an HM2000 and a Thornel 50 composite after ablation testing (Air Force Flight Dynamics Laboratory (AFFDL) 50MW).

The Thornel 50 multidirectional composites processed by high and low pressure procedures were examined at high magnification to determine the filament-matrix response when in the form of a composite. The composite

[9] F. R. Barnet and M. K. Norr, "Carbon Fiber Etching In An Oxygen Plasma," Carbon, Vol II, pp. 281-288 (1973).

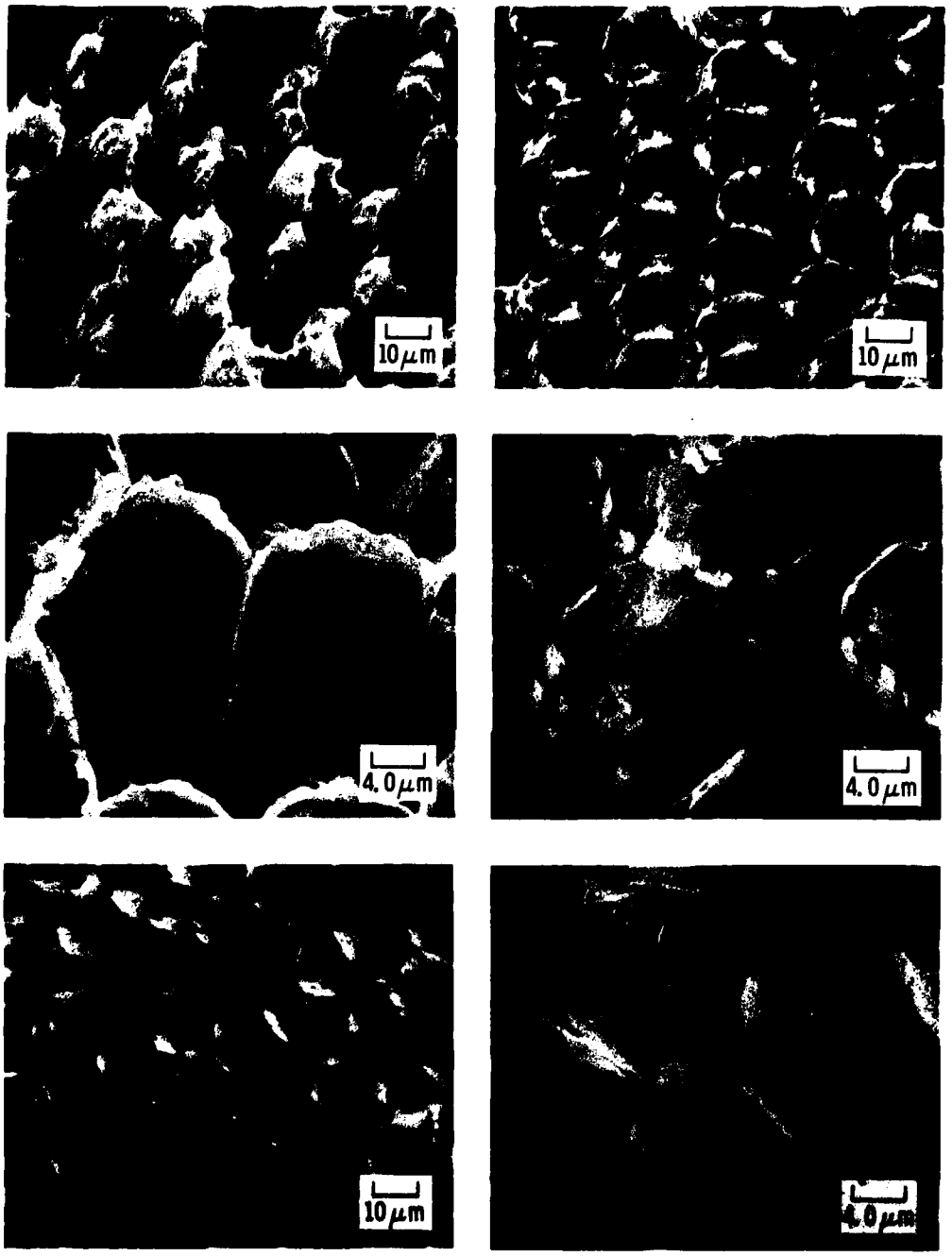

Figure 32. Scanning Electron Micrographs of Thornel 300 After Irradiation

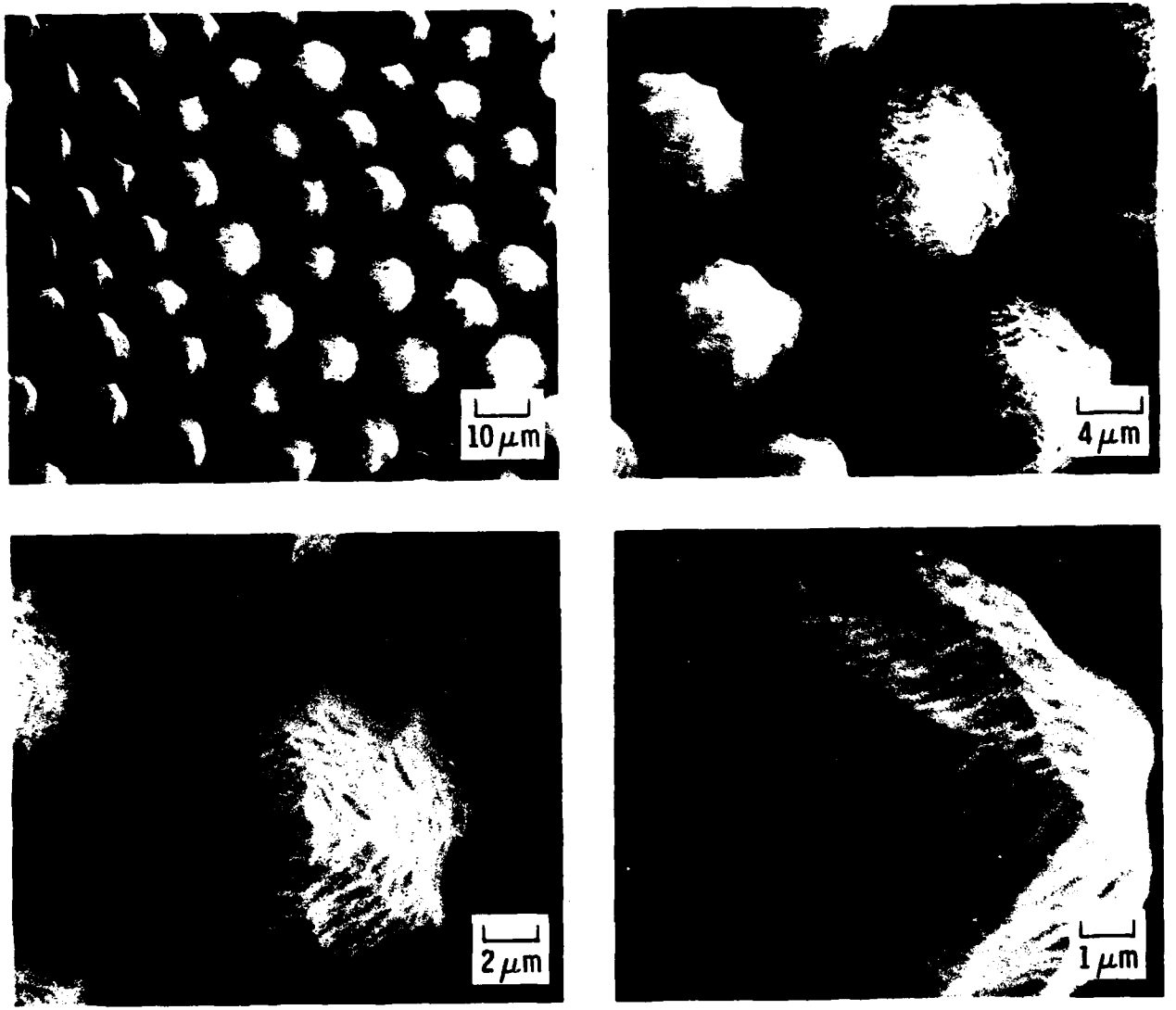

Figure 33. Scanning Electron Micrographs of Modmor 11 After Irradiation

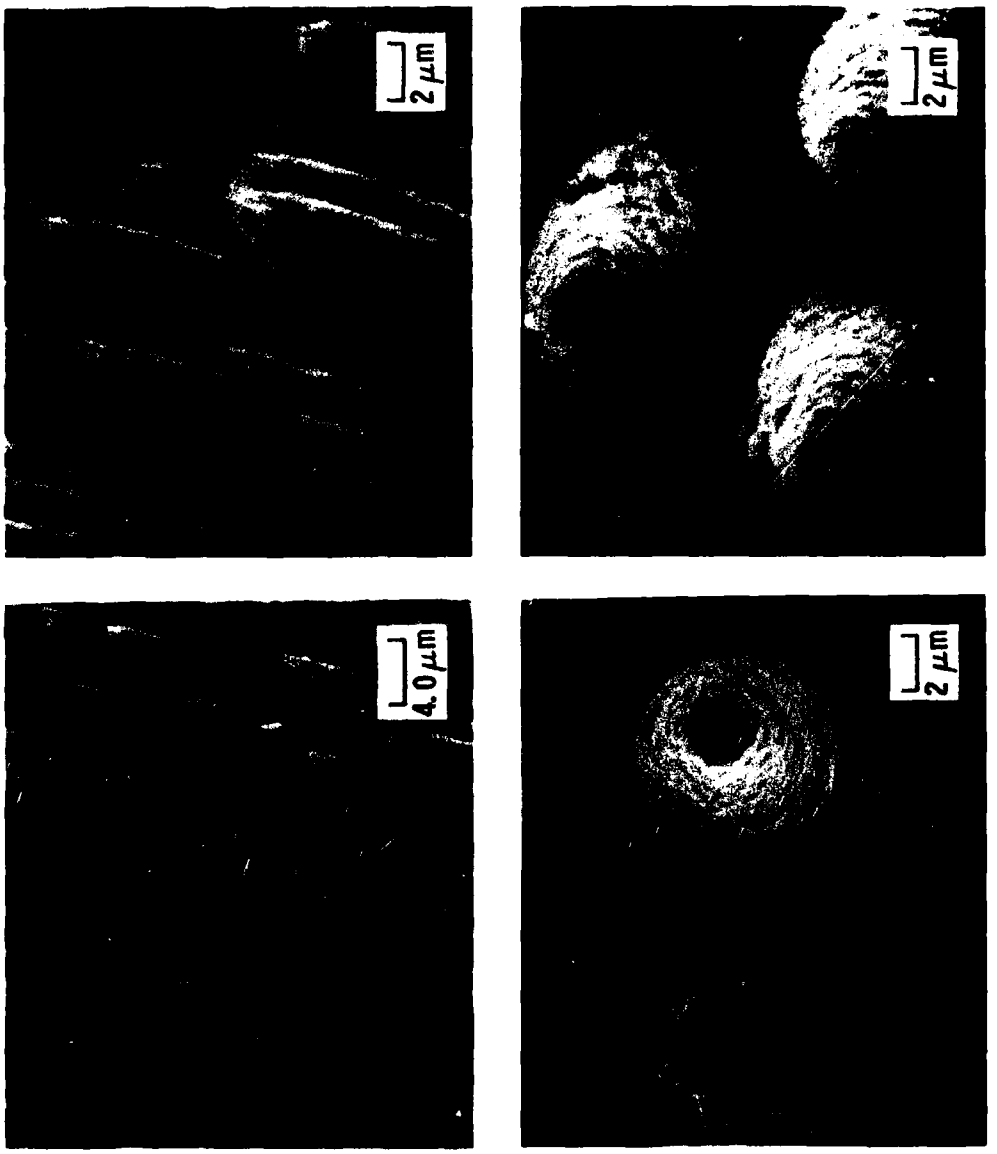

Figure 34. Scanning Electron Micrograph of HM2000 After Irradiation

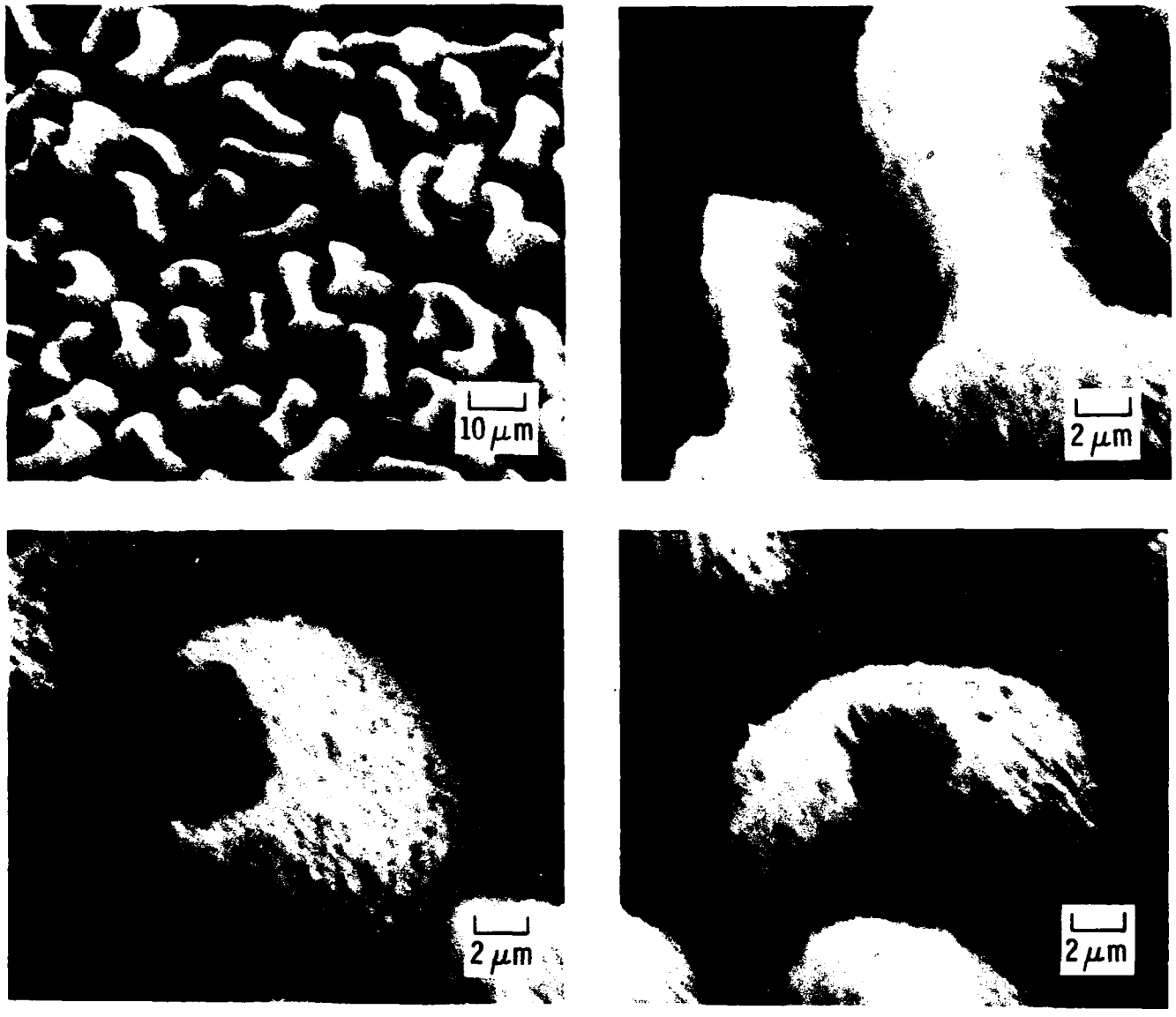

Figure 35. Scanning Electron Micrographs of GY70 After Irradiation

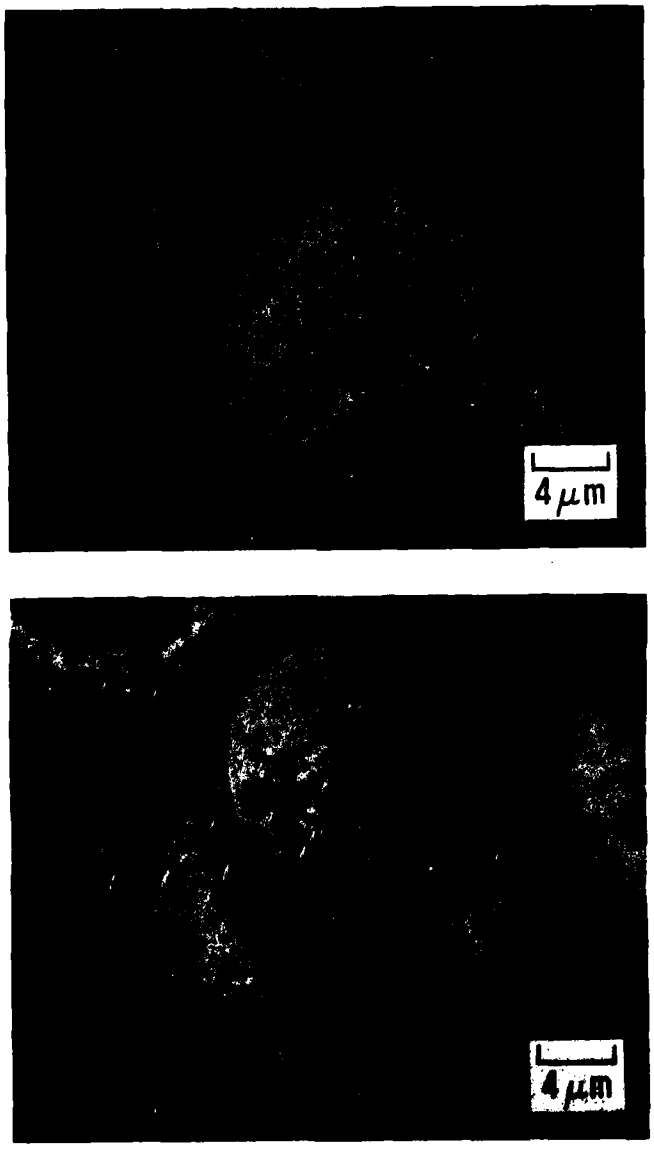

Figure 36. Scanning Electron Micrographs of Thornel P After Irradiation

processed by low pressure procedures (AX-1) is shown in Figures 39 thru 41. The filaments oriented parallel to the laser beam were flat or slightly slanted with the matrix phase being slightly more ablation-resistant (see Figure 39). The lack of tapered filaments as in the filament tests (see Figure 37) and in composite ablation tests (see Figure 38) may be due to the less severe environment. Flat Thornel 50 filaments were observed near the edges of the transverse craters for the bare filament experiments. For the filaments oriented normal to the laser beam, both filament and matrix can be found (see Figure 40). Also shown in Figure 40 is a filament fracture which could have occurred during the final graphitization step during processing. Although it could have occurred during the laser experiment, no other evidence of fracturing or microdamage could be found in the composite samples. The cross-sectional views through the crater did not reveal any evidence of mechanical damage in any of the constituents, filament ends, filament sides, or bulk matrix (see Figure 41). The transverse filament, bulk matrix, and longitudinal bundle (in order of decreasing recession) were similar to those observed during ablation testing. There was little difference between the bulk matrix and longitudinal bundles in either this experiment or in the ablation tests. This is consistent with the results discussed previously when the constituents were tested individually.

The microstructure of the multidirectional composite processed by high pressure procedures after laser irradiation is shown in Figures 42 thru 44. The filament ends and matrix receded at an equivalent rate with only a discontinuity at the filament-Chemical Vapor Deposition (CVD)-matrix interface (see Figure 42). At the interface it was apparent that the CVD receded at a faster rate than either the filament or matrix. At first glance one may conclude that the CVD offers no advantage since it erodes at a much faster rate than the other constituents. However, if by its recession it removes heat that would otherwise remove filament or matrix, it would be advantageous to have a CVD layer. The filaments oriented normal to the

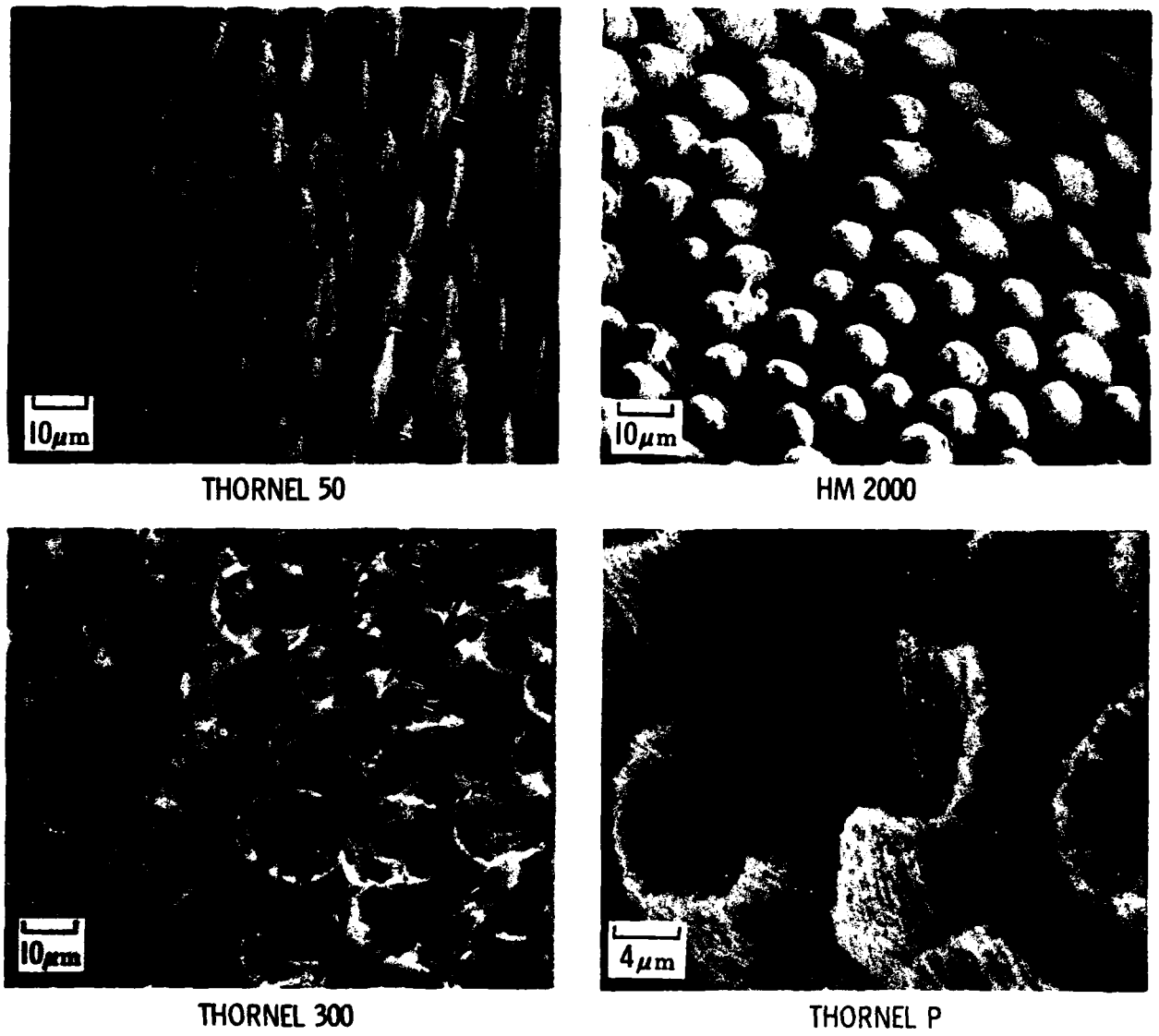

Figure 37. Filament Microstructure After Irradiation

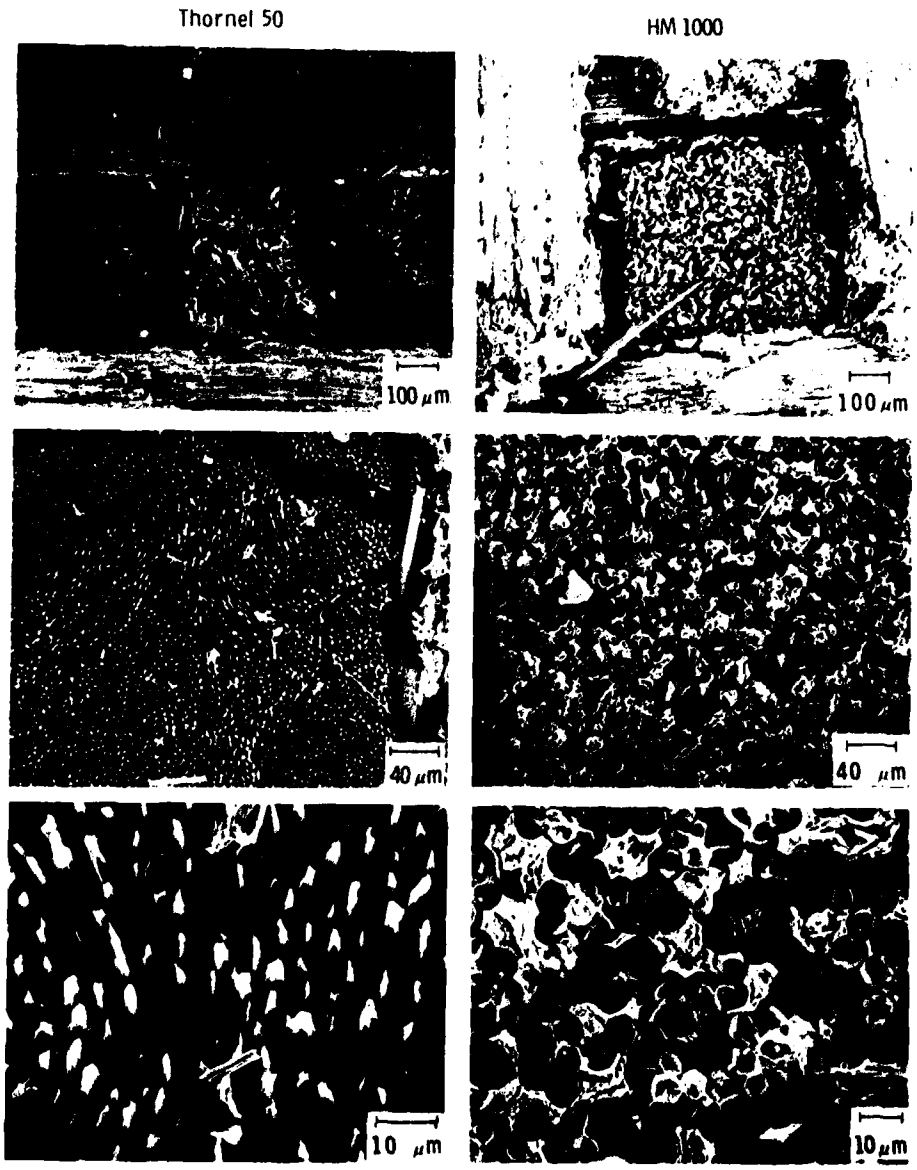

Figure 38. Scanning Electron Micrographs of Thornel 50 and HM2000 Composites After Ablation Testing

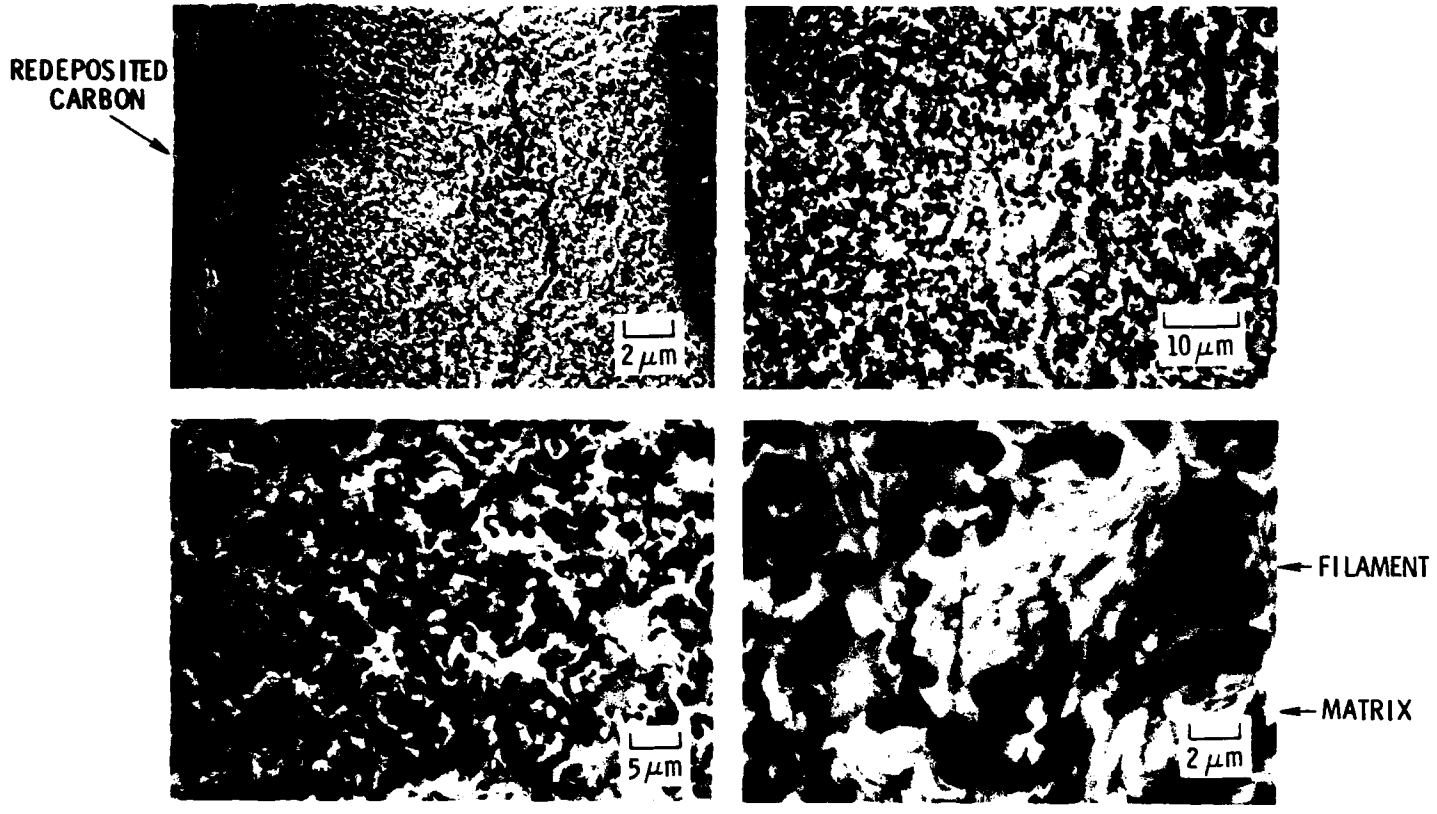

Figure 39. Scanning Electron Micrographs of Transverse Filament Bundle Composites Processed by Low Pressure Procedures After Irradiation

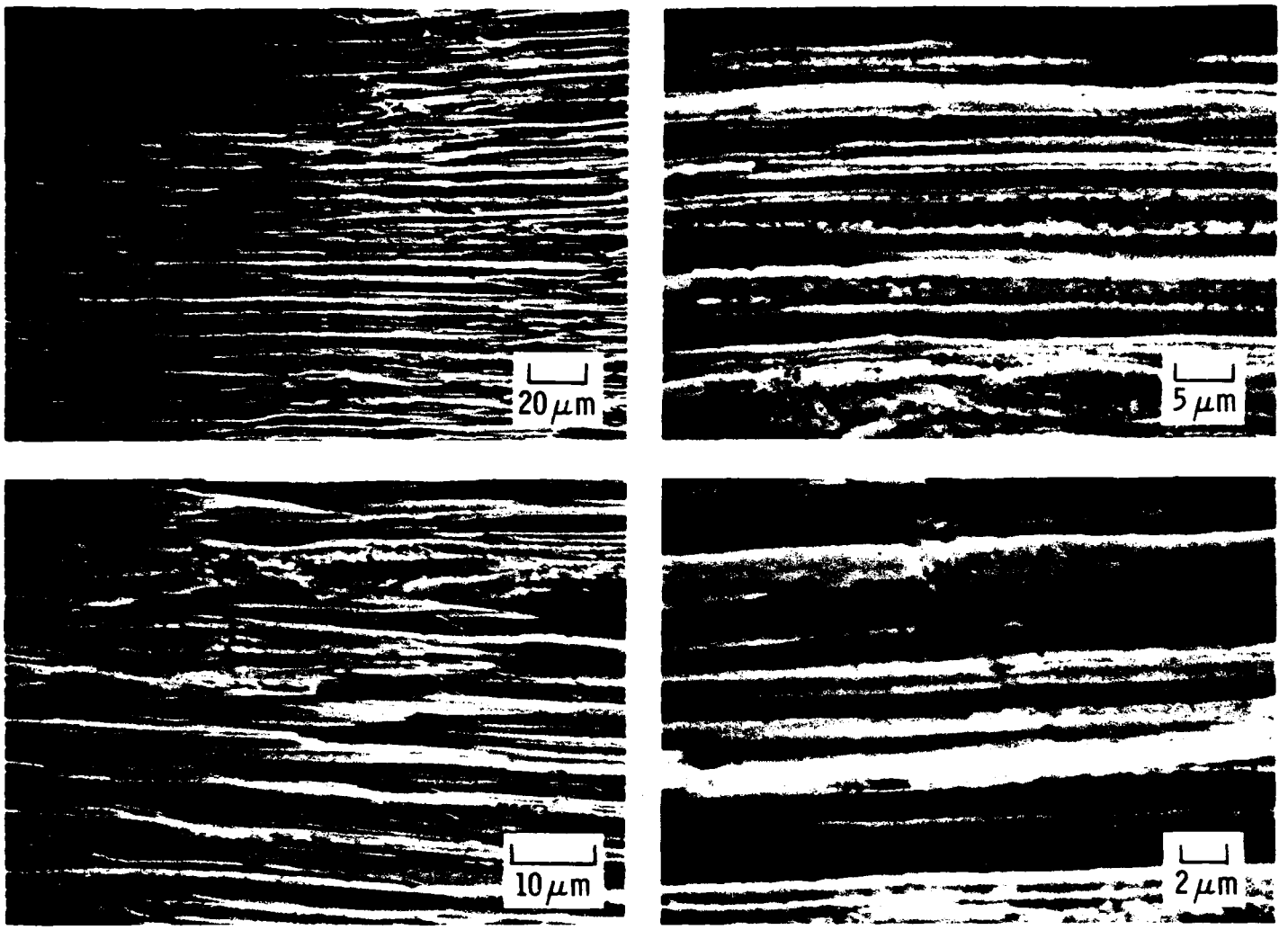

Figure 40. Scanning Electron Micrographs of a Longitudinal Filament Bundle Within a Composite Processed by Low Pressure Procedures After Irradiation

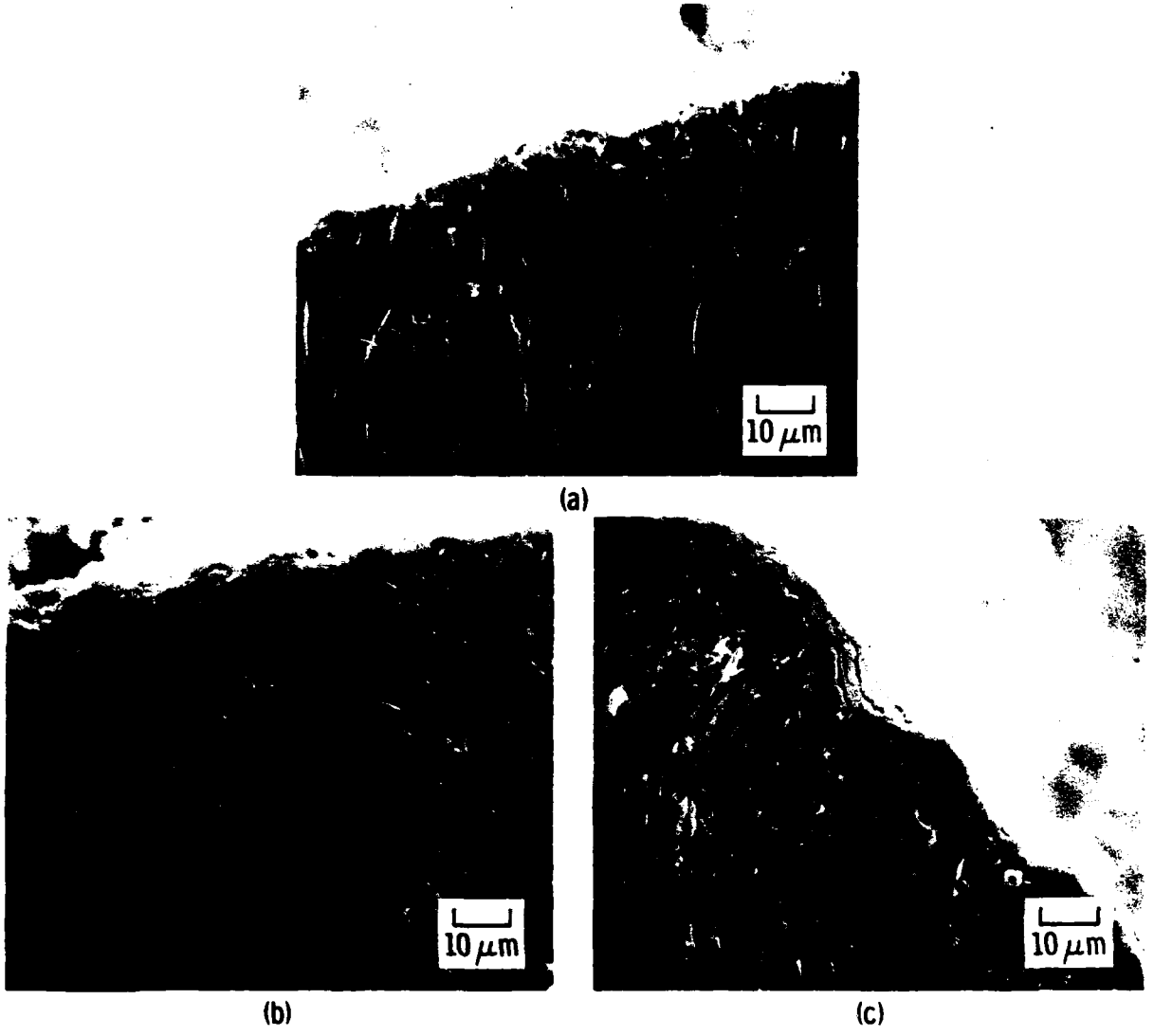

Figure 41. Scanning Electron Micrograph of Cross-Sectional Views of a Composite Processed by Low Pressure Procedures and Composite Components in the Crater

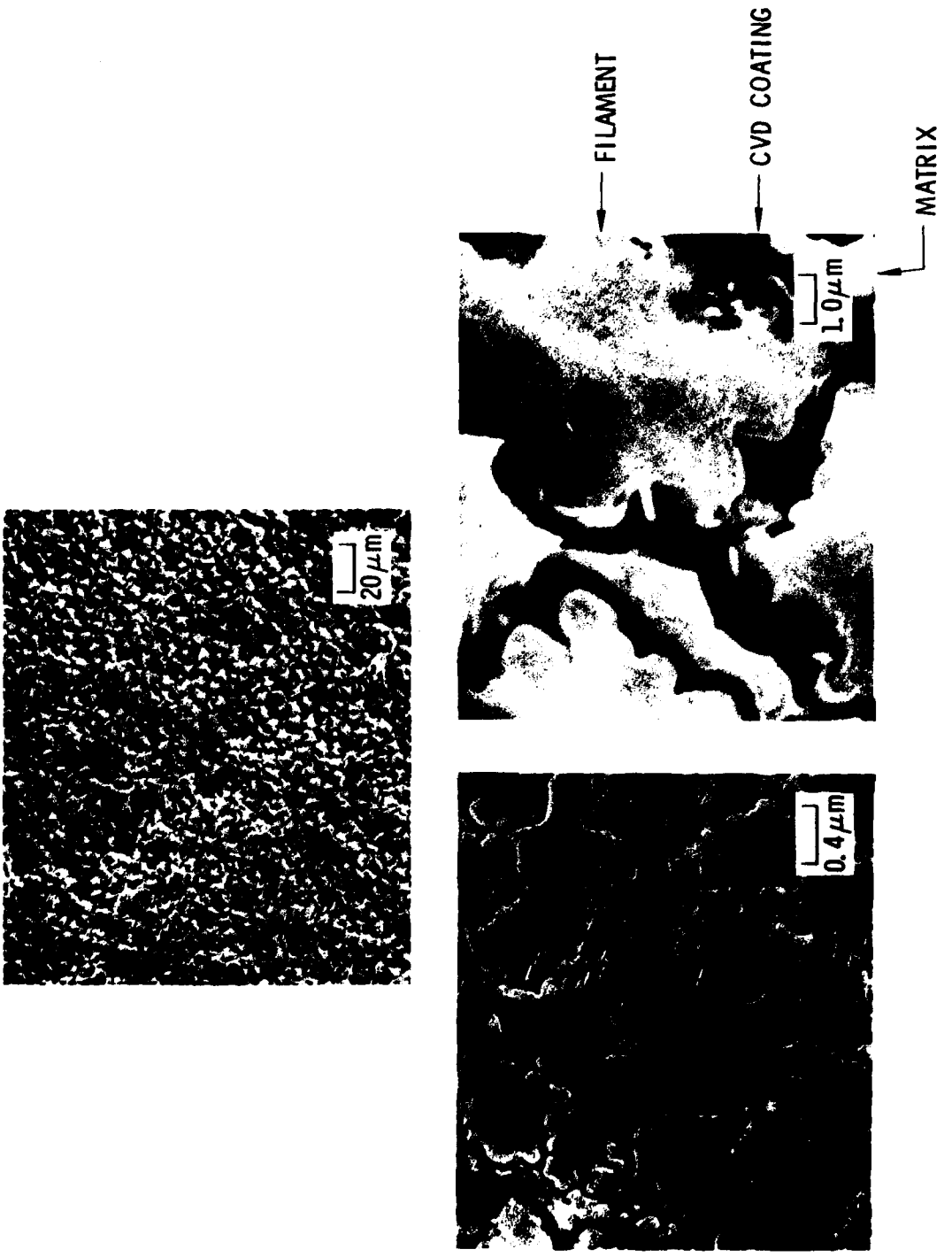

Figure 42. Scanning Electron Micrographs of a Transverse Filament Bundle Composite Processed by High Pressure Procedures After Irradiation

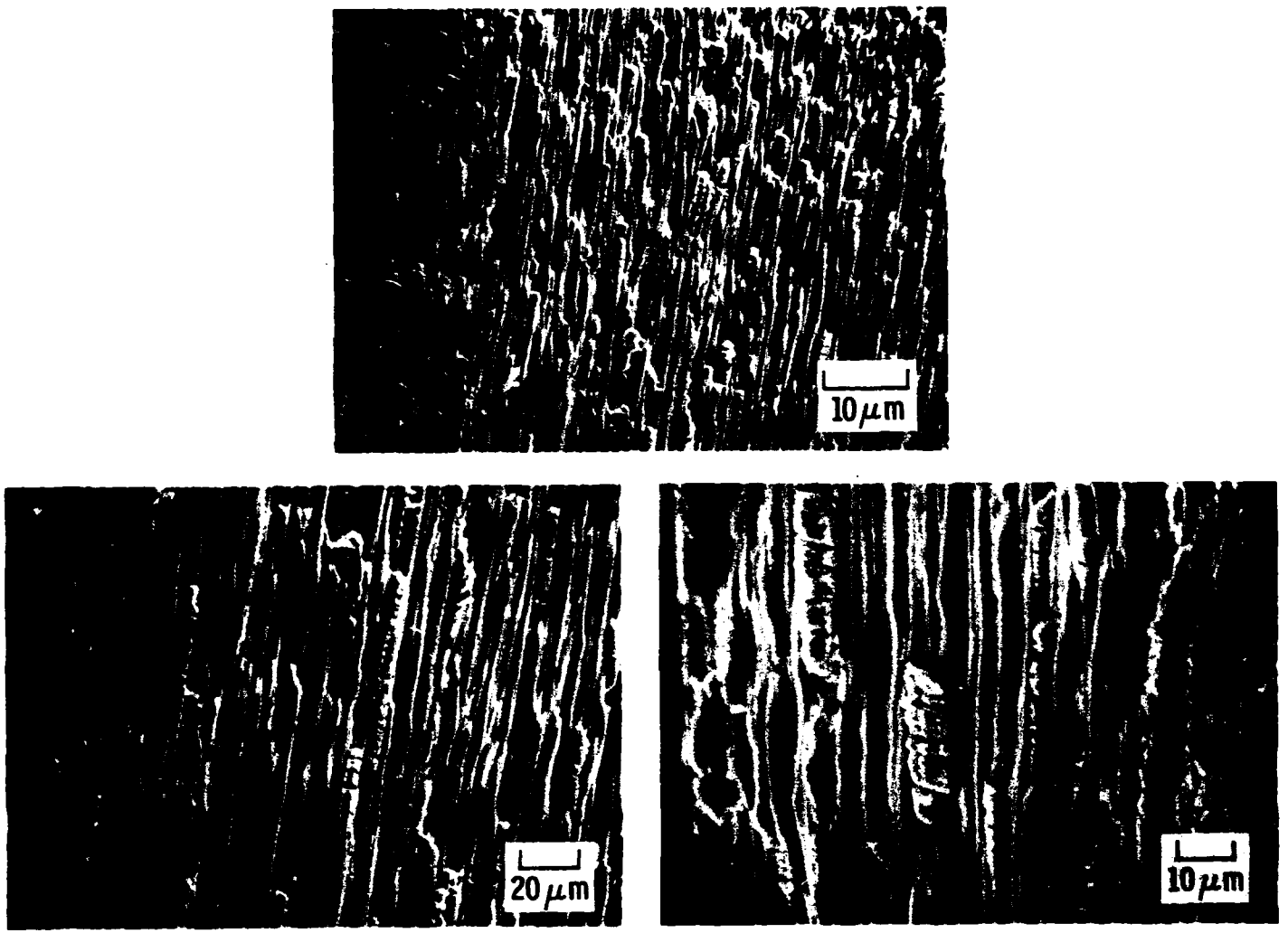

Figure 43. Scanning Electron Micrographs of a Longitudinal Filament Bundle Composite Processed by High Pressure Procedures After Irradiation

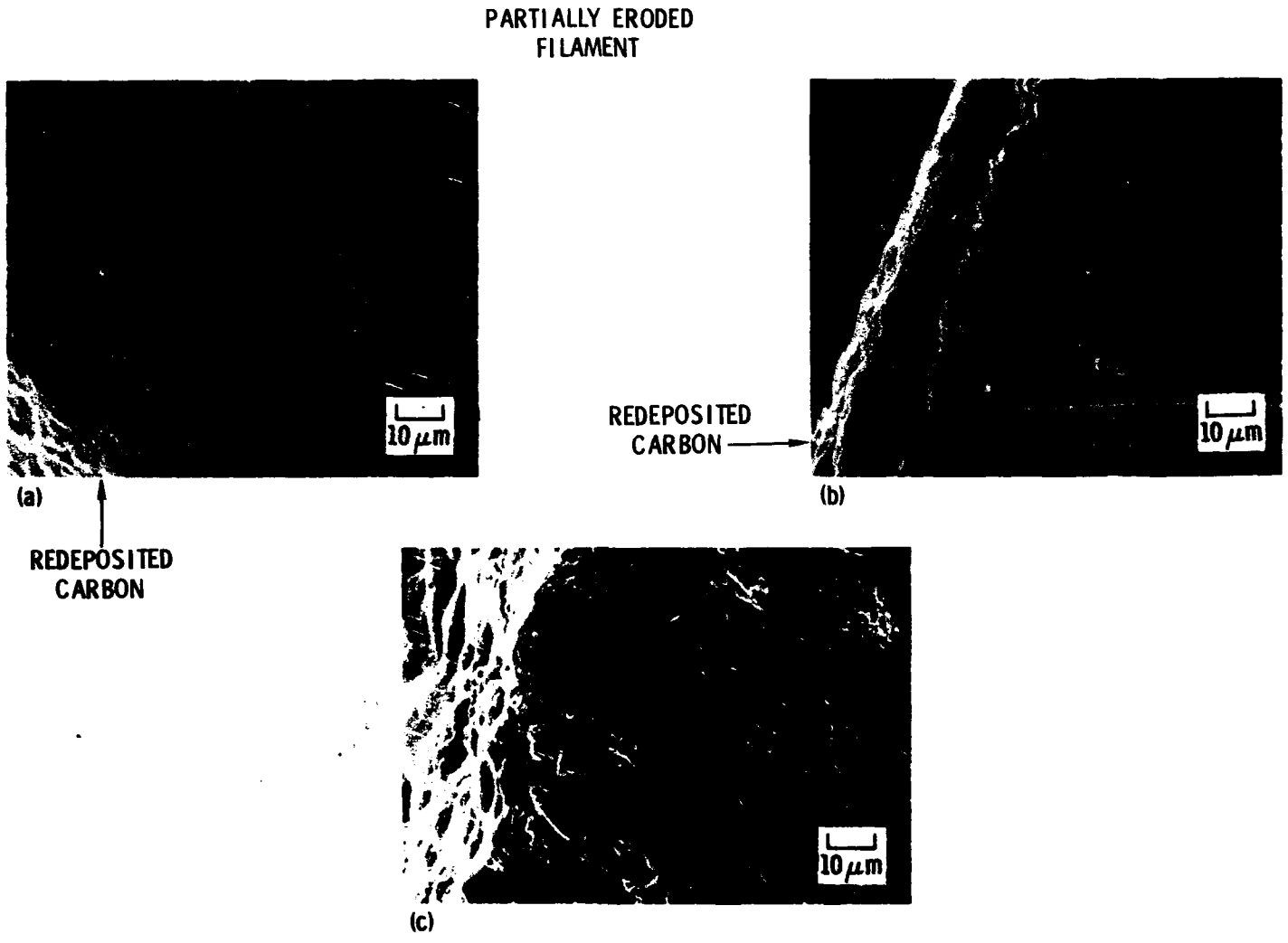

Figure 44. Scanning Electron Micrographs of a Composite Processed by High Pressure Procedures After Irradiation (a) and Cross-Sectional View of Carbonate Components in Crater (b), (c)

laser beam were more resistant than the matrix phase (see Figure 43). The transversely oriented inter-filament matrix is easily seen in this illustration. The fact that there is less matrix on the longitudinal filaments may be due to matrix recession being assisted by some mechanical removal as the CVD layer just below the matrix vaporizes. Unfortunately, there is no direct evidence for any mechanical removal; examination of the cross-sectional views of each constituent again shows no signs of mechanical failure. The top micrograph of Figure 44 shows filaments that have been partially eroded. Also, inter-filament matrix can be found adjacent to these eroded filaments.

These experiments have provided insight into the microstructural mechanisms of ablation and have shown that significant differences exist in the mass loss characteristics between constituents of carbon-carbon composites. The ranking of materials in order of decreasing mass loss was: transverse filament, longitudinal filament, bulk matrix, composites, and pyrolytic graphite. Significant differences were found in the transverse mass losses of filaments while the longitudinal mass losses were very close. Post-test macro/microstructures of the transverse filaments were also quite different for each filament. Strong correlations were found between mass loss, filament density, and modulus, and consequently, crystallographic orientation. However, one simple property alone did not control the mass loss characteristics. The mass loss characteristics of the three principal aerospace carbon filaments were equivalent.

The ranking of constituents from composite laser tests was similar to both the constituent laser tests as well as the AFFDL 50MW composite ablation tests. Since the lowest mass loss phases are 80 percent of the composite, they have a controlling effect on ablation. This implies that since the longitudinal filaments have a narrow range of mass losses, similar composites having different filaments can also be expected to have a narrow range of mass losses. The craters in the composites processed by high pressure

procedures were narrower and significantly deeper than the craters in composites processed by low pressure procedures. Further microstructural examination revealed that the CVD layer around the filaments recedes at a faster rate than either the filaments or matrix.

A brief carbon negative ion analysis was made of the coating that formed on the surface of the laser craters[10] (see Figures 12 and 13). In all cases, they were found to contain carbyne forms of carbon.[11] The amount of carbyne form remaining in the coating depends on two factors, namely, the rate of transformation of the graphitic carbon and the rate at which the coating was quenched. Qualitative results show that pyrolytic graphite transforms at a higher rate than binder carbon or glassy carbon. How the carbon fibers behave in this respect has not been determined. However, it is unlikely that they all transform at the same rate. The cooling rate of the coating will depend mostly upon radiation loss and on how fast heat can be conducted away from the coating. It was found that the carbynes were usually most prevalent in the coatings formed on the fiber sides. Since the radiation losses were much the same from craters formed in fiber sides and ends, it follows that conduction losses were greatest from craters formed on fiber sides. This conclusion is compatible with the geometry of the samples. For a single fiber, the direction of best thermal conductivity is along the fiber axis. Therefore, heat can be readily conducted away in two directions from a crater produced in the side of the sample. A crater produced in the fiber ends has only one direction of good conduction.

[10] W. K. Stuckey and A. G. Whittaker, "The Identification of Carbon Allotropes by Ion Microprobe Mass Analysis," Paper No. TP-177, Abstracts of the 10th Biennial Conference on Carbon, Bethleham, PA 278 (27 June - 2 July 1971).

[11] A. G. Whittaker, "Carbon: A New View of the High-Temperature Behavior of Carbon," Science (May 1978).

Specific results obtained from examination of some of the samples are listed below.

Thornel 50. Craters produced in both fiber directions had a high carbyne content, and this fiber appeared to produce a greater total amount of carbyne forms than any of the other fibers. Also, an unusual form of carbon (perhaps a carbyne) was found. This form gave only C^- and C_2^- signals and the C^-/C_2^- ratio was exceptionally high.

Thornel 75. Normal carbynes were found, but in low concentrations.

HM2000. Only the unusual carbon form (i.e., high C^-/C_2^- ratio) was found.

Thornel 300. Results were much like those for Thornel 75.

GY 70. Normal carbynes were found in a concentration that was intermediate between those of Thornel 50 and Thornel 75.

Thornel P. Normal carbynes were found, but in a low concentration as in Thornel 75.

WYB. This showed only the form of a high C^-/C_2^- ratio. A positive ion spectrum showed that this fiber was very low in inorganic impurities.

Modmor II. Normal carbynes in concentration similar to that in Thornel 75 were found.

All of the samples showed evidence of particle emission. The heating chamber was equipped with a tray to catch emitted material for analysis by the scanning electron microscope (SEM) and electron diffraction. A SEM search showed that most of the emitted material was composed of short segments and clusters of fibers. A few splats were found which indicated that the carbon was heated above its melting point ($\sim 3800°K$). Most of the electron diffraction patterns showed diffuse rings that are characteristic of graphitic carbon. A few clean single crystal patterns of chaoite were obtained.

VI. CONCLUSIONS

The laser irradiation experiments have shown that: (a) correlations exist between mass loss and materials properties, (b) significant differences in mass loss characteristics exist between the composite constituents and, (c) ablation testing results in similar correlations. It was concluded that laser irradiation of reentry nose tip materials can be used to screen candidate materials as well as to simulate an ablation environment. It is highly recommended that further testing be conducted on a variety of multi-directional carbon-carbon composites to obtain mass loss data, as well as to further the knowledge of composite ablation mechanisms. With such information, correlations between laser mass loss and ablation recession rates can be investigated.

Carbon negative ion spectra obtained from the material coating the laser craters showed that the carbon fibers transformed to carbyne forms of carbon during the heating cycle. The different types of fibers did not transform to the same extent.

Particle emission was observed in all cases and splats from liquid carbon were found in the emitted material. Electron diffraction patterns showed that most of the emitted material was graphitic, but a few single crystal patterns of chaoite were found.

APPENDIX. SUMMARY OF EXPERIMENTAL DATA

Specimen	Direction	Filament Volume Fraction, %	Weight Loss, %	Laser Power, kW	Irradiation Time, sec
WYB-28	Longitudinal	64	0.79	5.49	0.513
	Transverse		5.22	10.77	1.062
-29	Transverse	73	5.07	11.16	1.052
-30	Transverse	66	3.86	11.30	0.534
-31	Transverse	64	3.74	10.15	0.492
Thornel 50-5	Longitudinal	64	1.27*	11.76	0.534
	Transverse		3.85	11.17	1.048
-6	Longitudinal	70	1.04*	10.29	0.532
	Transverse		4.00	9.95	1.056
-7	Longitudinal	72	0.99	5.60	0.933
	Transverse		2.16	10.86	0.556
-8	Longitudinal	68	1.33	5.91	0.924
	Transverse		2.20	10.75	0.490
Thornel 75-17	Longitudinal	58	0.71	6.49	0.522
	Transverse		4.09	13.79	1.079
18	Longitudinal	51	0.74	6.04	0.507
	Transverse		4.08	10.78	1.162
-19	Transverse	57	1.90	9.76	0.525
-20	Transverse	58	0.85	10.24	0.539
Thornel 300-9	Longitudinal	73	1.40	10.12	0.535
	Transverse		3.53	10.53	1.060
-10	Longitudinal	73	1.48	10.64	0.500
	Transverse		3.31	9.26	1.036
-11	Longitudinal	74	1.36	5.44	0.968
	Transverse		2.35	11.15	0.569
-12	Longitudinal	75	1.19	6.30	0.748
	Transverse		2.12	10.30	0.530
Modmor II-13	Longitudinal	77	0.84	10.59	0.520
	Transverse		2.01	10.42	1.020
-14	Longitudinal	75	0.56	6.61	0.582
	Transverse		2.24	10.95	1.068
-15	Longitudinal	76	0.53	6.35	0.936
	Transverse		1.28	10.05	0.503
-16	Longitudinal	76	0.63	6.74	0.952
	Transverse		0.68	10.28	0.528
HM2000-1	Longitudinal	68	0.98	11.00	0.504
	Transverse		3.32	10.62	1.088
-2	Longitudinal	65	0.93*	11.12	0.550
	Transverse		3.22	10.88	1.030
-3	Longitudinal	66	0.98	6.34	1.002
	Transverse		2.96	10.49	1.030
-4	Longitudinal	68	0.99	6.06	1.000
	Transverse		2.19	11.91	0.590
-33	Transverse	64	1.56	10.58	0.499

*Beam hit metal holder, data discarded.

APPENDIX. SUMMARY OF EXPERIMENTAL DATA (Continued)

Specimen	Direction	Filament Volume Fraction, %	Weight Loss, %	Laser Power, kW	Irradiation Time, sec
GY 70-21	Longitudinal	57	0.68	5.74	0.495
	Transverse		4.00	10.77	1.090
-22	Longitudinal	67	0.99*	6.70	0.952
	Transverse		1.39	10.40	0.559
-23	Longitudinal	65	0.69*	6.07	0.891
	Transverse		2.25	10.94	0.510
Thornel P-24	Longitudinal	66	0.80	6.92	0.500
	Transverse		3.41	10.28	1.090
-25	Longitudinal	61	0.70	6.56	0.490
	Transverse		2.32	9.04	1.010
-26	Longitudinal	64	0.87	6.95	0.919
	Transverse		2.00	11.32	0.522
-27	Longitudinal	69	0.95	6.61	0.940
	Transverse		1.78	10.66	0.523
PG-1	c	-	0.13	6.45	0.969
	a		0.04	5.71	0.508
-2	c	-	0.13	5.56	0.984
	a		0.05	5.73	0.524
-3	c	-	0.13	4.89	0.914
	a		0.12	6.42	1.087
-4	c	-	0.07	5.22	0.506
	a		0.14	5.57	1.047
GE223 B1-1	z	-	0.21	6.27	0.504
-2		-	0.14	5.52	0.500
-1R		-	0.05	6.48	0.493
MDAC AX-1	z	-	0.17	6.02	0.554
-2		-	0.23	5.91	1.036
FMI221 B4-1	z	-	0.11	5.67	0.538
-2		-	0.07	5.33	0.986
GE223 D2-1	z	-	0.15	5.50	0.517
-2			0.14	5.82	0.500
HiPIC 1	-	-	0.11	5.83	0.500
7			0.24	6.57	1.036
MDAC LO 1	-	-	0.25	5.32	0.548
4			0.26	5.01	1.004

*Beam hit metal holder, data discarded.